









Cross-species evidence for a developmental origin of adult hypersomnia with loss of synaptic adhesion molecules *beat-1a/CADM2*

Received: 8 July 2024

Accepted: 22 December 2025

Published online: 12 January 2026

 Check for updates

Kyla Mace ^{1,2}, Amber Zimmerman^{2,3,4}, Alessandra Chesi ^{4,5}, Fusun Doldur-Balli ³, Hayle Kim ⁶, Erika Almeraya del Valle ², Jeffrey B. Rosa⁶, Allan I. Pack^{2,3}, Struan F. A. Grant ^{4,7,8,9} & Matthew S. Kayser ^{2,6,10} 

Idiopathic hypersomnia (IH) is a poorly understood sleep disorder characterized by excessive daytime sleepiness despite normal nighttime sleep. Combining human genomics with behavioral and mechanistic studies in fish and flies, we uncover a role for *beat-1a/CADM2*, synaptic adhesion molecules of the immunoglobulin superfamily, in excessive sleepiness. Neuronal knock-down of *Drosophila beat-1a* results in sleepy flies and loss of the vertebrate ortholog of *beat-1a*, *CADM2*, results in sleepy fish. We delineate a developmental function for *beat-1a* in synaptic elaboration of neuropeptide F (NPF) neurites projecting to the suboesophageal zone (SEZ) of the fly brain. Brain connectome and experimental evidence demonstrate these NPF outputs synapse onto a subpopulation of SEZ GABAergic neurons to stabilize arousal. NPF is the *Drosophila* homolog of vertebrate neuropeptide Y (NPY), and an NPY receptor agonist restores sleep to normal levels in zebrafish lacking *CADM2*. These findings point towards NPY modulation as a treatment target for human hypersomnia.

Disrupted sleep is associated with diverse negative physiological consequences^{1–3}. Over the past few decades, work in animal models and humans has led to new insights into genetic regulation of sleep^{4–7}, and more recent efforts have leveraged human genome wide association studies (GWAS) to examine the genetics of numerous sleep disorders^{8–10}. However, in contrast to disorders like sleep apnea and insomnia, few studies have focused on disorders of unexplained excessive sleepiness. Idiopathic hypersomnia (IH) is characterized by excessive daytime sleepiness despite normal nighttime sleep, often

accompanied by difficulty awakening (sleep inertia), unrefreshing sleep, and cognitive impairment (sleep drunkenness)^{11–13}. Unlike type 1 narcolepsy, a hypersomnolence disease whose pathophysiology is well-understood, the etiology of IH is opaque. This lack of knowledge contributes to underdiagnosis of IH and poor management of its symptoms¹⁴. Treatment strategies for this disorder have been hampered by a dearth of mechanistic insights. IH may be caused by heterogeneous etiologies, with hypothesized pathophysiologies relating to the immune system¹⁴, circadian clock^{15,16}, and GABAergic dysfunction¹⁷.

¹Pharmacology Graduate Group, Biomedical Graduate Studies, Perelman School of Medicine, University of Pennsylvania, Philadelphia, PA, USA. ²Chronobiology and Sleep Institute, Perelman School of Medicine, University of Pennsylvania, Philadelphia, PA, USA. ³Division of Sleep Medicine, Department of Medicine, Perelman School of Medicine, University of Pennsylvania, Philadelphia, PA, USA. ⁴Center for Spatial and Functional Genomics, Children's Hospital of Pennsylvania, Philadelphia, PA, USA. ⁵Department of Pathology and Laboratory Medicine, Perelman School of Medicine, University of Pennsylvania, Philadelphia, PA, USA. ⁶Department of Psychiatry, Perelman School of Medicine, University of Pennsylvania, Philadelphia, PA, USA. ⁷Department of Pediatrics, Perelman School of Medicine, Philadelphia, PA, USA. ⁸Divisions of Human Genetics and Endocrinology and Diabetes, Children's Hospital of Pennsylvania, Philadelphia, PA, USA. ⁹Department of Genetics, University of Pennsylvania, Philadelphia, PA, USA. ¹⁰Department of Neuroscience, Perelman School of Medicine, University of Pennsylvania, Philadelphia, PA, USA. ✉e-mail: kayser@penmedicine.upenn.edu

Yet, mechanistic evaluation of these or other hypotheses remains limited.

Regardless of underlying cause, IH has a heritable component: twin studies show that daytime sleepiness is between 37–48% heritable and family history of excessive sleepiness is present in ~1/3 of IH patients^{11,18–20}. Recent GWAS focused on sleep and circadian rhythms have provided new insights into sleep in health and disease⁵. Discerning the biological impact of implicated loci remains a challenge, as little is known of their functional effects, due in part to the often-erroneous assumption that the nearest gene is the causal effector gene²¹. Non-coding regions of the genome contain important regulatory elements and genetic variants that disrupt those elements can confer susceptibility to complex disease; such regulatory elements can be at substantial distance from the actual effector gene. “Variant-to-gene” mapping approaches have been applied to identify functional effects of variants emerging from insomnia GWAS, followed by validation in animal models⁸. However, even these approaches can fail to fully account for potential genes impacted by a given variant. For example, a regulatory variant is more likely to affect expression in cis of a gene within its topologically associated domain (TAD) rather than elsewhere in the genome²². A TAD is defined by Hi-C approaches as a self-interacting genomic region²². As such, DNA regions within a TAD physically interact with each other more frequently than with regions outside the TAD^{23,24}. Prioritizing candidate genes within TADs has allowed for the identification of distal disease genes²⁵, but such a comprehensive approach has never been applied to sleep traits.

Here, combining human genomics with behavioral and mechanistic studies in fish and flies, we investigate molecular and genetic underpinnings of hypersomnia. Using a full TAD-wise analysis of genome wide significant loci associated with hypersomnia traits, we conducted a reverse-genetic screen in *Drosophila* to implicate candidate effector genes. This screen revealed a role for the synaptic adhesion molecule *beat-la* and its vertebrate ortholog, *CADM2*, in excessive sleepiness, coinciding with the napping and daytime sleepiness GWAS locus on human chromosome 3. Detailed analyses in flies support a developmental role for *beat-la* in coordinating synaptic elaboration of wake-promoting neuropeptide F (NPF) neurites in the suboesophageal zone (SEZ) of the fly brain. Loss of *beat-la* disrupts NPF synaptic input to GABAergic targets in the SEZ, resulting in impaired ability to maintain wakefulness. NPF is the *Drosophila* homolog of vertebrate neuropeptide Y (NPY) and we find that an NPY receptor agonist restores normal sleep/wake balance to zebrafish lacking *CADM2*, demonstrating how cross-species approaches may uncover novel treatment targets for human hypersomnia.

Results

Identification and RNAi screen of candidate hypersomnia-associated genes

To identify molecular and genetic factors contributing to excessive sleepiness, we conducted a reverse-genetic knockdown screen of hypersomnia-associated genes (Fig. 1 for schematic). The most comprehensive GWAS for sleep reported to date is based on the UK Biobank ($n = 452,071$) where 243 loci were identified^{26,27}. Using objective data about sleep in a subset of participants with 7-day accelerometry, 24 loci were initially associated with sleep propensity (excessive sleep duration, daytime napping, and daytime sleepiness), although 59 other loci were associated with sleep fragmentation, presumably secondarily driving daytime sleepiness and therefore less relevant to IH^{26–28}. Additionally, the first GWAS of IH patients ($n = 414$) revealed 4 loci specifically associated with IH²⁹. With the goal of investigating the sleep propensity loci as exhaustively as possible, we identified all genes residing within the corresponding TADs harboring each GWAS signal from the 28 sleep propensity and hypersomnia loci identified. For this analysis, we used TAD coordinates from neural progenitor cells

derived from the human HI NPC line²². This approach resulted in 26 TADs harboring 511 human genes, 274 of which are protein coding, coinciding with sleep propensity GWAS signals (Fig. 1A, Supplementary Data 1).

Using DIOPT, an integrated ortholog prediction tool that combines numerous algorithms³⁰, we identified 231 fly orthologs for these human genes, and 376 publicly-available RNAi lines targeting the fly genes (Fig. 1A). We then screened sleep parameters in flies with expression of individual RNAi under control of the pan-neuronal driver, *elav-GAL4* (Fig. 1B). Because male flies show substantially more daytime sleep than female flies, we conducted our screen using females to avoid potential ceiling effects masking long sleep phenotypes. Sleep in each RNAi genotype was normalized against an RNAi control for the given experiment to control for inter-experimental differences. This screen revealed numerous RNAi lines whose pan-neuronal expression increased sleep duration (Fig. 1C). Enriched among long-sleepers were members of the *beaten path* family of genes, which were predicted to be homologs of human *CADM2*. *CADM2* is a gene within the same TAD as the non-coding variant, rs1601550, which has been reported to be associated with both excessive daytime sleepiness and daytime napping in humans²⁶ (Fig. 1D). We chose to focus on a single gene, *beat-la*, for which two independent RNAi increased sleep duration greater than 2 standard deviations of the mean.

Neuronal knockdown of *beat-la* increases sleep without affecting locomotor activity

CADM2 and *beat-la* are members of the immunoglobulin containing superfamily, functioning as synaptic adhesion molecules with known roles in neural circuit wiring^{31–34}. We first replicated our findings from the screen with a larger sample size, yielding a consistent increase in sleep duration during both day and night in *beat-la* knockdown flies (Fig. 2). We also validated that both *beat-la* RNAi effectively knockdown mRNA expression in brain (Supplementary Fig. 1A) and that the long sleep phenotype is replicated in males (Supplementary Fig. 1B–K). Excess sleep in *beat-la* knockdown flies was driven by an increase in sleep bout length, suggestive of more consolidated sleep (Fig. 2F, I). These initial experiments were conducted in *Drosophila* activity monitors (DAMs) utilizing a single infrared beam to detect periods of sleep, so we next assessed sleep phenotypes with *beat-la* RNAi using a higher spatial resolution multi-beam sleep assay as well as additional parental controls. We found again that neuronal knockdown of *beat-la* resulted in increased sleep duration during the day and night (Supplementary Fig. 2). Importantly, in both single- and multi-beam analyses, we detected no reduction of locomotor activity during periods of wake in *beat-la* knockdown animals (Fig. 2B, Supplementary Fig. 2C, F), confirming that increased sleep is not a confound related to altered motor function. Finally, co-expressing *beat-la* cDNA in the context of *beat-la* RNAi attenuated the long sleep phenotype (Supplementary Fig. 3), providing further evidence that the increase in sleep is specific to loss of *beat-la*.

Other synaptic cell adhesion molecules have been implicated in sleep regulation³⁵, and *beat-la* is one member of the *beaten path* family of synaptic adhesion factors³⁶. To determine whether neuronal knockdown of other *beat* family members likewise affects sleep, we re-examined candidates from our initial human-informed screen. Indeed, we observed sleep phenotypes with knockdown of other *beat* isoforms, including increased sleep from *beat-Ic* and *beat-VII* knockdown; and decreased sleep from *beat-Ib*, *beat-IIIc*, and *beat-Vb* knockdown (Supplementary Fig. 4). For mechanistic studies, we focused on *beat-la* as this phenotype was most robust and reproducible. Moreover, knockdown of *beat-la*'s putative receptor *sidestep*^{37,38} (Fig. 3) or the transcription factor *SoxN*³⁹ (Supplementary Fig. 5) known to regulate *beat-la* expression recapitulates the hypersomnia phenotype, strongly implicating the *beat-la* signaling pathway in sleep.

Fig. 1 | A reverse-genetic screen of hypersomnolence-associated variants identifies *beat-1a* as a sleep regulatory molecule. **A** Schematic of gene candidate nomination and sleep screen in *Drosophila*. **B** Total sleep across 24 h of flies expressing RNAi driven by pan-neuronal *elav-GAL4*. *UAS-Dcr2* was co-expressed for RNAi of the *VALIUM1* or *VALIUM10* vector to improve RNAi efficacy. Sleep duration for each experimental genotype was normalized to the control genotype of the experiment in which it was run. Bars indicate the mean of sleep measurements from 8-16 animals, except for 3 RNAi lines which have 3-7 animals each. **C** Normalized total sleep for longest sleeping lines (> 2 standard deviations from the mean of all animals). Members of the *beaten path* family of immunoglobulins, predicted homologs of human *CADM2*, are highlighted. Each datapoint represents one

animal. Bar plots display mean \pm SEM. All sleep experiments were run with single-beam DAM monitors. Source data are provided as a Source Data file. **D** Top: Topologically associated domain containing the GWAS association signal for putative sleep propensity loci (in neural progenitor cells). TAD coordinates were retrieved from 3D Genome Browser (HI-NPCs) (<http://3dgenome.fsm.northwestern.edu/index.html>). Genes in black are on + strand, genes in blue are on - strand. Bottom: Locus zoom plots of the chromosome 3 region associated with napping and daytime sleepiness retrieved from the Sleep Disorder Knowledge Portal (<https://sleep.hugeamp.org/>). Lead SNP for napping rs1601440 is indicated by the orange line. Nearest gene is *LINCO0971* (non-coding). Nearest protein coding gene is *CAMD2* (see TAD). LD (EUR) is indicated by color for sentinel SNP rs1601440.

to a sleep state from wakefulness. Notably, the elevation in sleep duration in these animals might occlude the ability to detect any further increased probability of entering a sleep state, since the flies are much less commonly awake to begin with.

Next, we empirically tested other sleep propensity measures. We assessed arousal threshold as a measure of sleep depth and found that *beat-1a* animals were less likely to be awoken by a stimulus during sleep in comparison to controls, during both the day and night (Fig. 4A). Given that individuals with hypersomnia exhibit difficulty staying awake and rapid transition to sleep, we also examined whether *beat-1a* knockdown animals similarly fall asleep more quickly than controls. We measured latency to sleep after animals first wake in the morning after lights turn on (ZT0). Typically, control flies first return to sleep ~120 min after morning awakening; in contrast *beat-1a* RNAi flies exhibited a first sleep bout in less than half that time (Fig. 4B). Recent work in flies has also demonstrated that long sleep bouts reflect deeper sleep stages⁴¹, so we next assessed sleep comprised of long bouts (> 60 min) with *beat-1a* knockdown (Fig. 4C). We found that *beat-1a* knockdown animals spend a greater percentage of time in long sleep bouts than controls, suggesting more time spent in deeper sleep.

Finally, circadian dysregulation has been proposed as a mechanism of human IH. However, we observed no change to any measure of locomotor rhythms in *beat-1a* flies under constant darkness (Fig. 4D-E), indicating that circadian function is unaffected and does not account for the sleep phenotypes. We also examined the response to sleep deprivation and found sleep homeostasis to be intact in *beat-1a* knockdown animals (Supplementary Fig. 7A,B). Although *beat-1a* knockdown animals display less recovery sleep than controls (Supplementary Fig. 7C), this may be due to a ceiling effect as *beat-1a* flies already sleep excessively during the day. Taken together, loss of *beat-1a* is associated with not only excessive sleep duration, but also numerous other sleep propensity phenotypes similar to those observed in human hypersomnia.

***beat-1a*'s ortholog, *CADM2*, regulates sleep in zebrafish**

beat-1a was identified as an ortholog of vertebrate *CADM2*. While *beats* and *CADM2* are not structurally similar, they are functionally similar: both are synaptic adhesion factors of the immunoglobulin superfamily, and both are critical for axon pathfinding^{31,33,34,36,42,43}. We next tested whether vertebrate *CADM2* has a role in sleep regulation by disrupting its expression in zebrafish (*Danio rerio*), a model of vertebrate sleep⁴⁴⁻⁴⁷. Using CRISPR/Cas9 gene editing in F0 larvae followed by automated video sleep tracking^{8,48}, we generated exonic mutations of critical regulatory domains, predicted to produce loss-of-function through frameshifts in *cadm2b*, the most conserved transcript (Supplementary Fig. 8). We then screened larvae for sleep phenotypes beginning at 5 days post fertilization (dpf), comparing *cadm2b* knockout zebrafish to control zebrafish (scrambled gRNA-injected) larvae. *cadm2b* knockout increased daytime and nighttime sleep, without an effect on activity, similar to sleep with *beat-1a* knockdown in *Drosophila* (Fig. 4F-I). These findings support the hypothesis that *CADM2* regulates vertebrate sleep.

***beat-1a* acts during development to regulate adult sleep**

Previous studies of *beat-1a* have focused on its role patterning the larval neuromuscular junction³⁴. In development, *beat*-expressing motor neurons follow a path of muscle, glial, and neuronal tissue marked by its receptor side^{37,38,49}. In *beat-1a* or *side* null mutants, motor axons fail to defasciculate from the axonal bundle and do not innervate their muscular targets³⁴. *beat-1a* null mutants are pre-adult lethal, preventing mutant analysis of adult sleep and suggesting that knockdown, as opposed to complete loss of expression, uncovers previously unknown adult roles. Although unlikely given the lack of locomotor phenotypes with pan-neuronal *beat-1a* knockdown (see Fig. 2, Supplementary Fig. 2), we next asked whether the adult sleep phenotype might be related to the canonical role for this protein in motor neurons. Expression of *beat-1a* RNAi under control of any of three well-characterized motor neuron GAL4 drivers failed to increase sleep (Fig. 5A-B), further supporting the hypothesis that *beat-1a* acts elsewhere to regulate adult sleep.

We then tested whether *beat-1a* is acting in development or adulthood to control adult sleep. We used a ubiquitously expressed temperature sensitive GAL4 repressor (*tubGAL80ts*)⁵⁰ to restrict *beat-1a* knockdown to pre- or post-eclosion. First, we limited knockdown of *beat-1a* to the pre-eclosion developmental period and then assessed sleep in adulthood. Developmental loss of *beat-1a* was sufficient to cause the excessive sleep phenotype (Fig. 5C-E). In contrast, limiting *beat-1a* knockdown to adulthood using two independent approaches had no effect on sleep (Fig. 5C-E, Supplementary Fig. 9). Together, these findings demonstrate *beat-1a* acts in a developmental capacity to cause excess sleepiness later in life.

***beat-1a* functions in neuropeptide F (NPF) cells to regulate sleep**

Our data raise the possibility of a role for *beat-1a* signaling outside of the neuromuscular junction. Given that *beat-1a* is necessary in development for normal adult sleep, we hypothesized that it is involved in patterning adult sleep circuits, presumably in the brain. First, we showed with qPCR that *beat-1a* is expressed in the brain (Supplementary Fig. 1A). To define the neuronal subpopulations in which *beat-1a* acts to regulate sleep, we conducted a targeted spatial knockdown screen, driving *beat-1a* RNAi in cells known to have a role in sleep or circadian behavior. We expressed *beat-1a* RNAi in relevant neurotransmitter and neuropeptide populations, clock cells, and other sleep-implicated neuronal populations with GAL4s that express during the developmental time period (larval/pupal) in which *beat-1a* is acting (Fig. 6A, Supplementary Fig. 10). Of the lines screened, we observed increased sleep when driving *beat-1a* RNAi in cholinergic cells using ChaT-GAL4 compared to an RNAi control. We also observed a trend toward increased sleep when driving *beat-1a* RNAi in neuropeptide F (NPF) cells using NPF-GAL4. ChaT-GAL4 expresses broadly throughout the fly nervous system, and we found expression overlap with NPF-GAL4 (Supplementary Fig. 10G). Although we cannot rule out the possibility that *beat-1a* signaling in other cells could contribute to adult sleep phenotypes, we focused on a role in NPF-expressing neurons given that NPF-GAL4 labels a

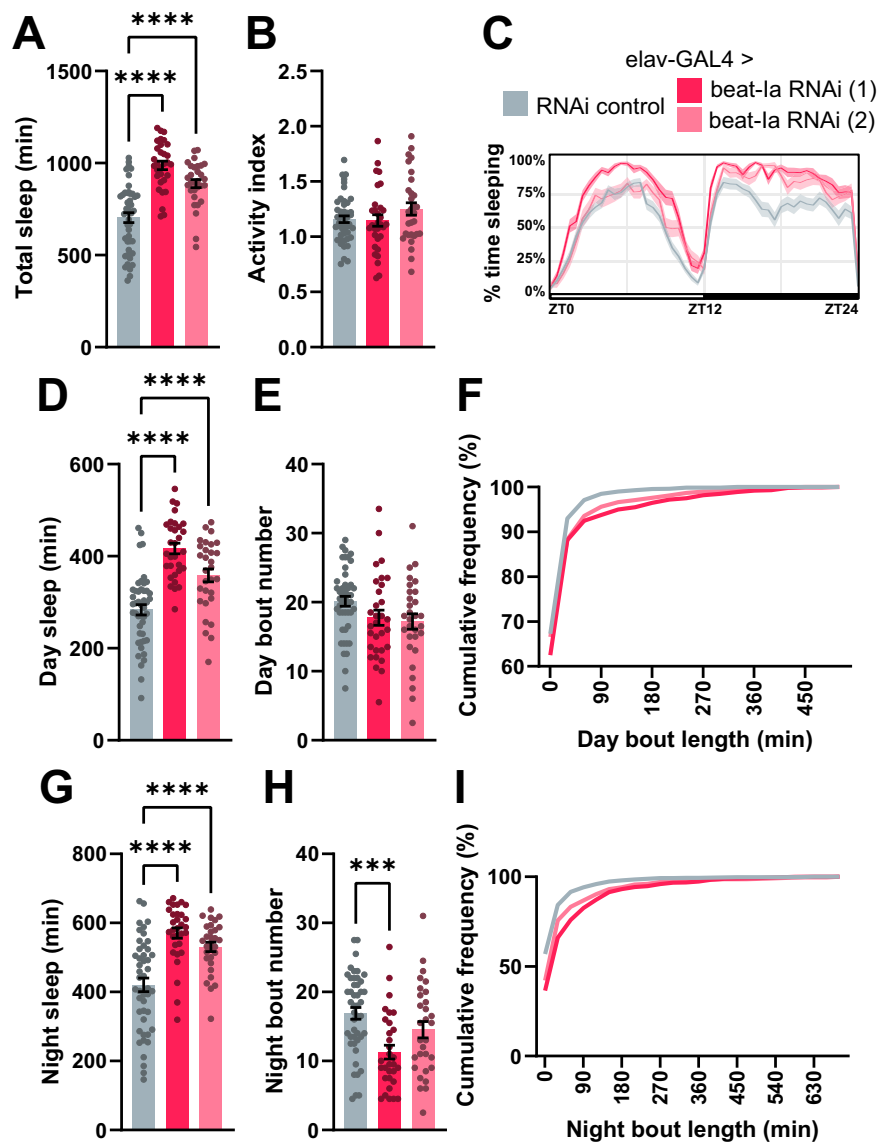


Fig. 2 | Pan-neuronal knockdown of *beat-1a* increases sleep duration without disrupting locomotor activity. Sleep measures for flies expressing either an RNAi control or RNAi against *beat-1a* in all neurons. **A** Total sleep duration across 24 h. **B** Activity index, which represents the number of infrared beam breaks per minute of waking activity. **C** Sleep trace depicts sleep amount (%) in rolling 30 min bins across day (ZT0-12, light) and night (ZT12-24, dark). **D** Average daytime sleep duration. **E** Average number of daytime sleep bouts. **F** Cumulative frequency plot of the relative frequency of daytime sleep bouts of increasing duration. **G** Average

nighttime sleep duration. **H** Average number of nighttime sleep bouts. **I** Cumulative frequency plot of the relative frequency of nighttime sleep bouts of increasing duration. Sleep experiments were run with single-beam DAM monitors. One-way ANOVA with Dunnett's multiple comparisons tests comparing experimental genotypes to control. *n*, from left to right = 46, 31, 30. *** $p \leq 0.001$, **** $p \leq 0.0001$. Each datapoint represents one animal. Bar plots display mean \pm SEM. Source data are provided as a Source Data file.

relatively sparse population of cells with a known sleep regulatory role⁵¹⁻⁵³.

Following the initial candidate screen, we replicated the NPF results using higher spatial resolution sleep monitoring and additional controls, which confirmed a strong excess sleep phenotype (Fig. 6B-K). As in pan-neuronal *beat-1a* RNAi flies, knockdown in NPF cells was not only associated with increased day and night sleep (Fig. 6D, H), but also prolonged sleep bouts (Fig. 6G, K). Importantly, we observed no decrease in locomotor activity (Fig. 6E, I). Analysis of long sleep bouts, a proxy for deeper sleep⁴¹, revealed a dramatic increase in this type of sleep during day and night (Fig. 6L-N). Given that NPF cells are sexually dimorphic, we tested NPF *beat-1a* knockdown in males; however, the high baseline sleep in males precluded our ability to detect an increase in sleep (Supplementary Fig. 11). Overall, *beat-1a* RNAi expression in NPF cells

appears to recapitulate sleep features observed with pan-neuronal knockdown.

NPF cells have a known role in sleep and feeding, among other behaviors in the fly. Previous work has shown that activation of NPF cells can promote wakefulness and feeding, and that these functions are dissociable: specific NPF neuronal subpopulations promote wakefulness without affecting feeding, and vice versa⁵². We hypothesized that the increase in sleep in NPF>*beat-1a* RNAi animals is due to a loss of a wakefulness-promoting cue. Alternatively, NPF>*beat-1a* RNAi animals could experience altered feeding behavior or nutrient storage, leading to disrupted energy homeostasis and an indirect effect on sleep. However, NPF>*beat-1a* RNAi flies showed no defects in feeding or nutrient storage as measured by the Capillary Feeding Assay and a starvation resistance assay⁵⁴ (Supplementary Fig. 12), supporting a specific developmental role for *beat-1a* in NPF arousal circuitry.

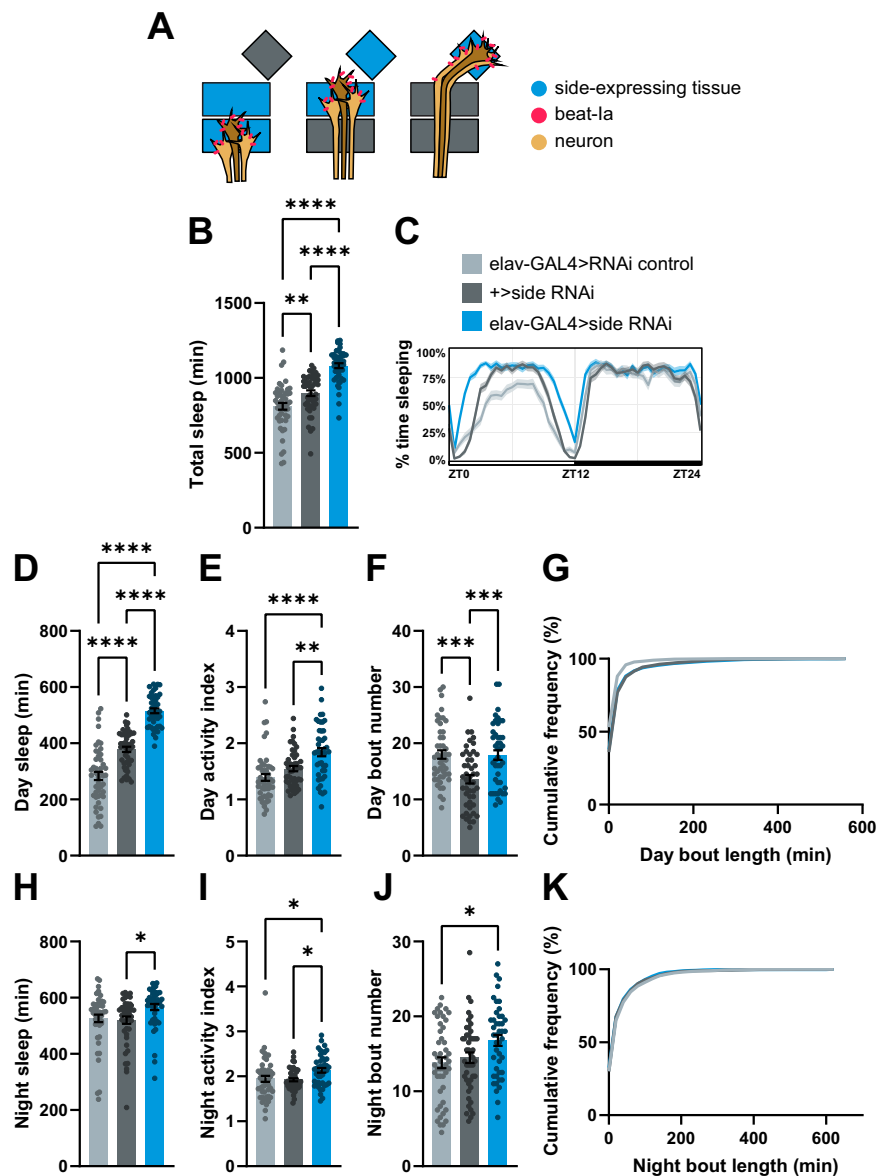


Fig. 3 | Pan-neuronal knockdown of *beat-1a*'s receptor, *side*, produces a long sleep phenotype. **A** Schematic of the *beat-1a* signaling pathway, illustrating how *beat-1a*-expressing neurons follow a path of tissue (glia, muscle, neural, and epithelial) marked by its receptor *side*. Adapted from Siebert et al. 2009. **B** Total sleep duration across 24 h. **C** Sleep trace. **D–G** Day sleep measures. **H–K** Night sleep

measures. Sleep experiments were run with single-beam DAM monitors. One-way ANOVA with Tukey's multiple comparisons test comparing all genotypes to each other. *n*, left to right = 48, 47, 44. * $p \leq 0.05$, ** $p \leq 0.01$, *** $p \leq 0.001$, **** $p \leq 0.0001$. Each datapoint represents one animal. Bar plots display mean \pm SEM. Source data are provided as a Source Data file.

beat-1a coordinates NPF neuronal synaptic development in the subesophageal zone (SEZ)

To determine how loss of *beat-1a* affects NPF wiring, we first used NPF-GAL4 to co-express membrane-bound GFP (UAS-CD8::GFP) with *beat-1a* RNAi or an RNAi control. Surprisingly, we observed no changes in NPF cell body number or neurite morphology/location (Fig. 7A). NPF cells have dense dendritic and axonal projections, precluding assessment of more subtle morphological effects using this approach. Given that *beat-1a*'s known neuronal function is presynaptic, we next labeled presynaptic sites using EGFP tagged Synaptotagmin (Syt-EGFP). While co-expression of *beat-1a* RNAi had no detectable impact on most regions where NPF cells send projections, we noted a dramatic loss of synaptic density in the subesophageal zone (SEZ) of the fly brain (Fig. 7B). *beat-1a* knockdown significantly reduced the size of Syt-EGFP-labeled NPF synapses in the SEZ (Fig. 7C), likely due to the complete loss of characteristic C-shaped clusters of synapses found in control

brains (Fig. 7D). Closer examination of axonal projections confirmed that NPF axons reach the SEZ and appear morphologically normal (Fig. 7A, inset), and we failed to detect an overall change in synaptic puncta with analysis of the whole brain, arguing against broad NPF circuit dysregulation (Fig. 7E). These findings suggested a defect in synaptogenesis or synaptic maintenance in NPF projections to the SEZ with loss of *beat-1a*. We therefore assessed when NPF neurons normally innervate the SEZ. Imaging of NPF>Syt-EGFP brains across pupal development, we found elaboration of NPF neuronal presynaptic sites in the SEZ occurs during mid- to late-pupal development (Supplementary Fig. 13A–B). Knockdown of *beat-1a* specifically during pupal stages was sufficient to increase sleep in adulthood (Supplementary Fig. 13C–G), further supporting a role for *beat-1a* in NPF synapse elaboration during this time.

Implication of the SEZ-projecting NPF neurons in wakefulness was unexpected, as the lateral, Cry⁺ NPF cells have been best characterized

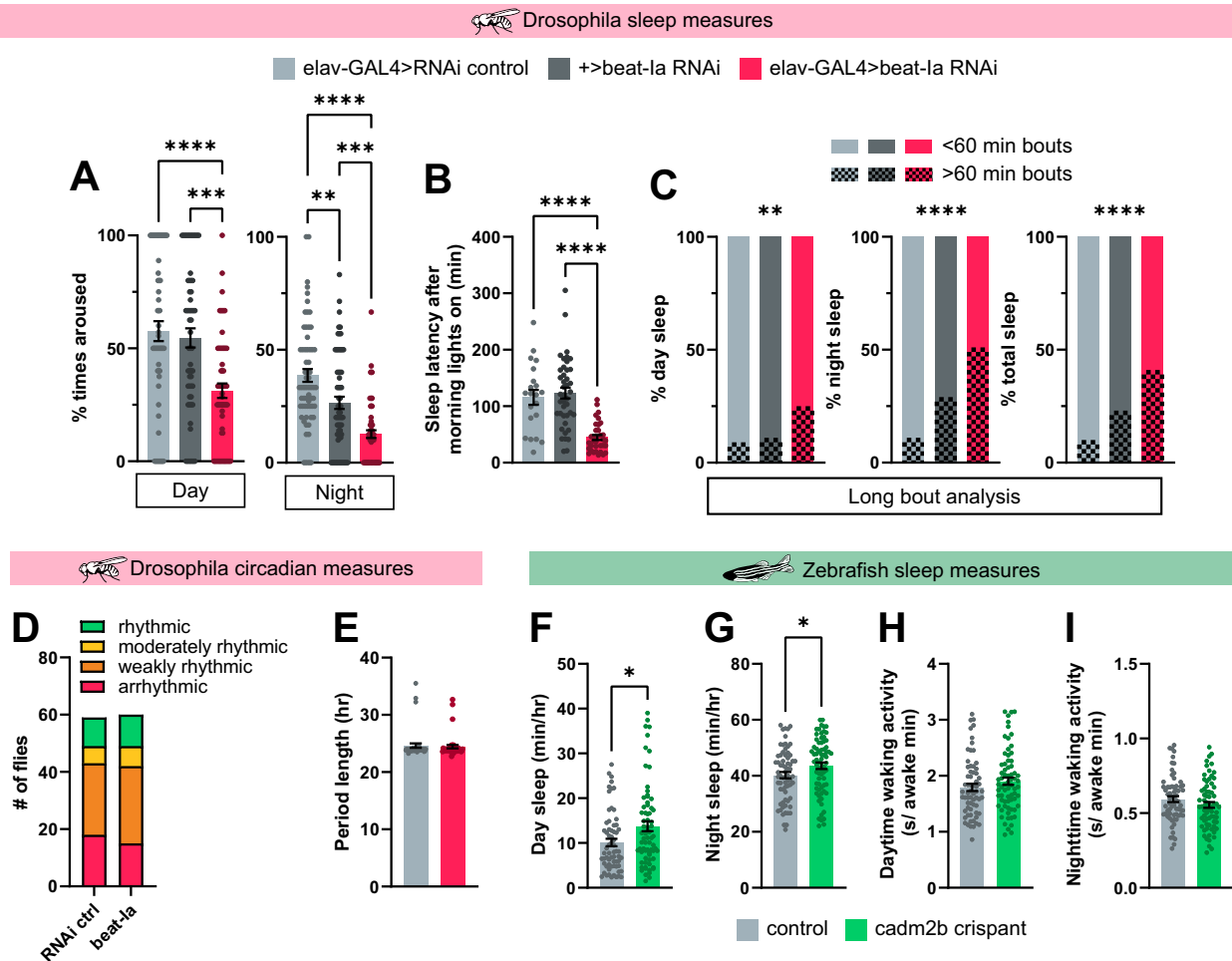


Fig. 4 | Increased sleep duration and measures of sleep propensity with loss of *beat-la* in flies and *cadm2b* in fish. **A** Daytime and nighttime arousal threshold (% of flies woken from sleep with a uniform stimulus). One-way ANOVA with Tukey’s multiple comparisons test comparing all genotypes. *n*, from left to right = 63, 63, 64. **B** Sleep latency following awakening at lights-on. One-way ANOVA with Tukey’s multiple comparisons test comparing all genotypes. *n*, from left to right = 21, 42, 34. **C** Proportion of day, total, and night sleep spent in long (> 60 min) vs. short (< 60 min) sleep bouts. Fisher’s exact test, two-sided. **D, E** Analysis of rest:activity rhythms in *beat-la* RNAi vs controls: **D** Number of animals categorized as

arrhythmic to rhythmic under constant dark conditions. *n*, from left to right = 59, 60. Chi-square test, ns. **E** Length of circadian periods in animals under constant conditions. Arrhythmic animals were excluded from analysis. *n*, from left to right = 42, 45. Unpaired t test, ns. Sleep experiments were run with single-beam DAM monitors (**B, D–E**) or multibeam DAM monitors (**A, C**). **F–I** Sleep measures for control and *cadm2b* crispant zebrafish. **F** Mann-Whitney test, two-tailed. **G** Unpaired t test, two-tailed. *n*, from left to right = 65, 71. * *p* ≤ 0.05, ** *p* ≤ 0.01, *** *p* ≤ 0.001, **** *p* ≤ 0.0001. Each datapoint represents one animal. Bar plots display mean ± SEM. Source data are provided as a Source Data file.

in this role⁵². We therefore identified a split-GAL4 that expresses exclusively in the descending NPF-SEZ cells and found that activation of these neurons indeed promotes wakefulness during the day (Supplementary Fig. 14). In addition, we noticed reduced Syt-EGFP signal in the dorsal fan-shaped (dFB) body of some *beat-la* knockdown brains; the dFB has a well-established role in sleep regulation^{55–59}, leading us to ask whether disruption of dFB innervation could be related to the sleep phenotype with *beat-la* knockdown. Quantification of dFB Syt-EGFP revealed no significant difference between control and *beat-la* knockdown animals, despite variability in this region of *beat-la* RNAi brains (Supplementary Fig. 15A–B). Nonetheless, to further probe a potential role for the dFB in the *beat-la* sleep phenotype, we assessed whether knockdown of the NPF receptor (*NPFR*) in these cells might be associated with increased sleep (Supplementary Fig. 15C–L). *NPFR* knockdown in dFB sleep cells failed to recapitulate the long-sleep phenotype found in NPF>*beat-la* RNAi animals, providing further evidence that changes in dFB function are unlikely to be involved.

Finally, given that *beat-la* knockdown in NPF cells impairs synapse development and adult wakefulness, we examined whether *beat-la*

overexpression might yield the opposite phenotypes. We found that expression of UAS-*beat-la* along with Syt-EGFP in NPF neurons resulted in a dramatic increase in presynaptic sites across many areas of the brain, including SEZ (Fig. 8A–B). Moreover, *beat-la* overexpression flies exhibited a decrease in total and daytime sleep (Fig. 8C–L), as well as a reduction in long sleep bouts (Fig. 8M–O), providing further evidence that *beat-la*-directed NPF synaptic development tunes sleep-wake balance in adulthood.

Identification of putative downstream sleep-regulatory cells in the SEZ

If loss of NPF synaptic innervation in the SEZ causes excess sleep in *beat-la* knockdown animals, then presumably NPF cells are synapsing onto sleep-regulatory SEZ targets. What are the downstream neuronal targets that would have received NPF input if not for loss of *beat-la*? Using FlyWire, a publicly available *Drosophila* connectome dataset^{60,61}, we identified 22 candidate cells that receive input from either of the descending NPF neurons (SLP.AVLP.4 and SLP.AVLP.5, in FlyWire) and have input regions in the SEZ (“gnathal ganglion” in the FlyWire

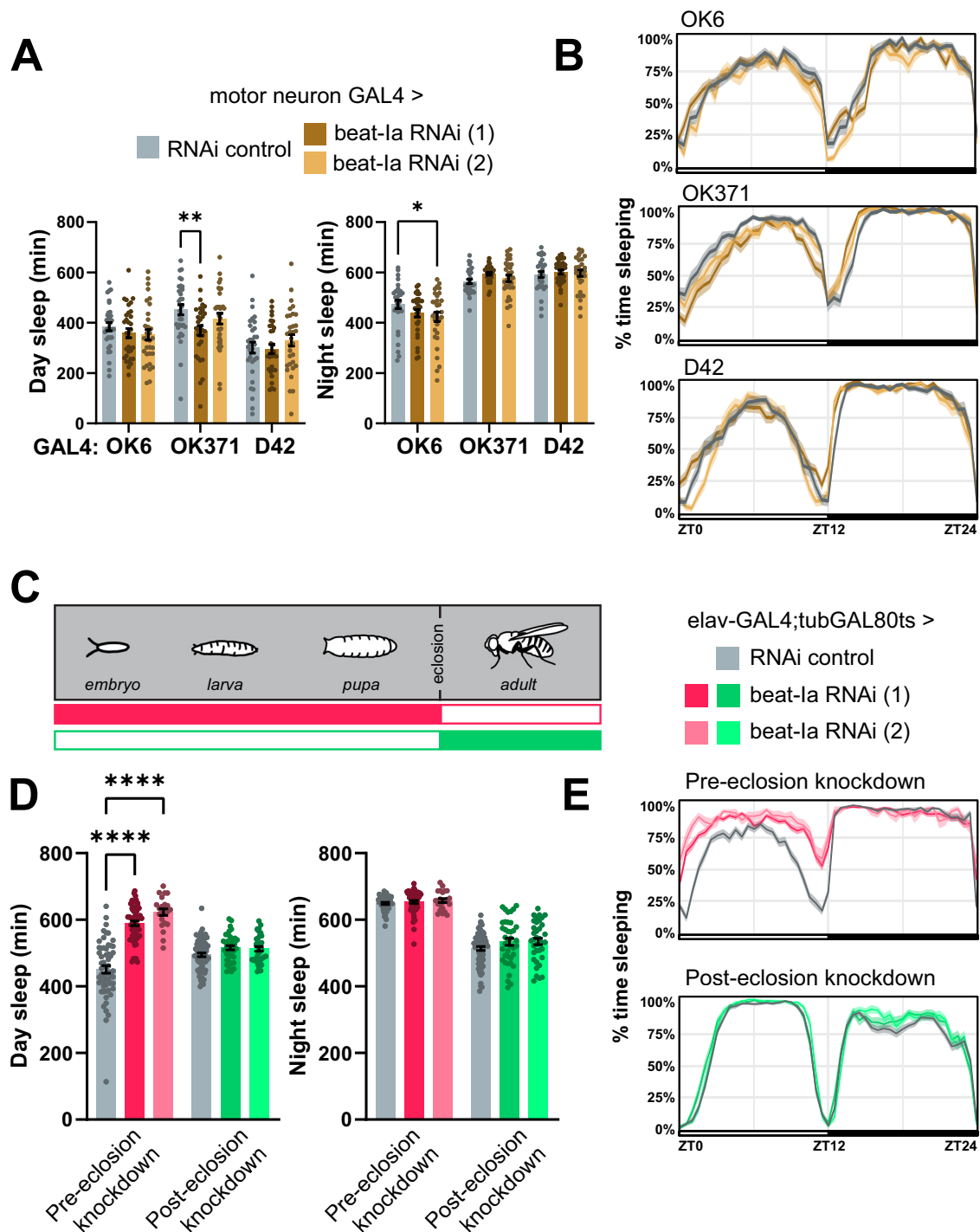
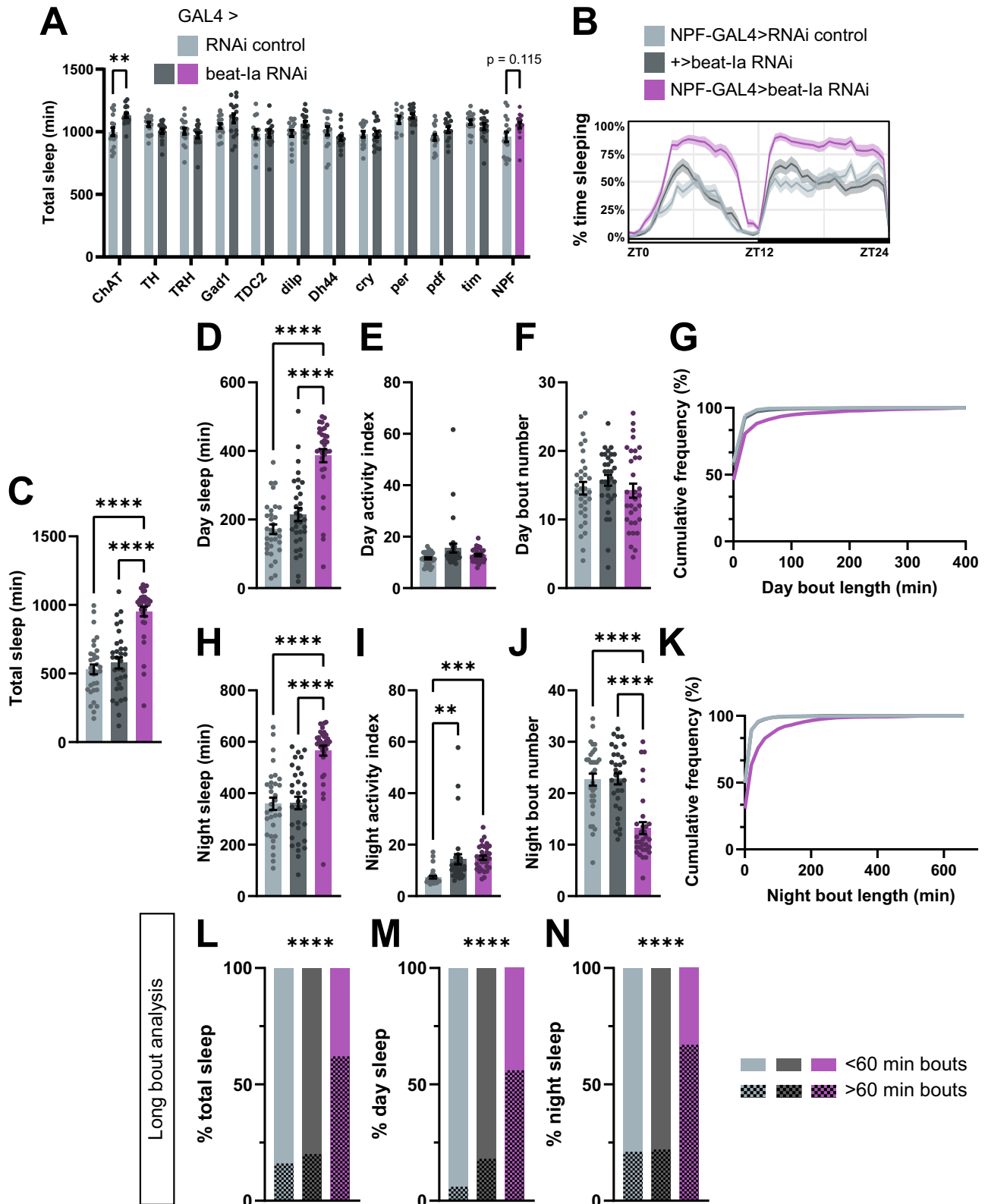


Fig. 5 | *beat-la* acts in development to regulate adult sleep. Day and night sleep duration (A) and sleep traces (B) from flies expressing *beat-la* RNAi under motor neuron drivers. Two-way ANOVA with Dunnett's multiple comparisons tests comparing experimental genotypes to control. *n*, from left to right = 32, 31, 31, 32, 31, 28, 32, 31, 30. C Schematic of temporal restriction of *beat-la* knockdown using a temperature sensitive ubiquitously expressed GAL4 repressor (*tubGAL80ts*). Day and night sleep duration (D) and sleep traces (E) from flies in which neuronal *beat-la* is

knocked down in development or adulthood. Sleep experiments were run with single-beam DAM monitors. Two-way ANOVA with Šidák's multiple comparisons tests comparing experimental genotypes to control. *n*, from left to right = 52, 33, 10, 57, 38, 32. * $p \leq 0.05$, ** $p \leq 0.01$, **** $p \leq 0.0001$. Each datapoint represents one animal. Bar plots display mean \pm SEM. Source data are provided as a Source Data file.

dataset) (Fig. 9A). Using BrainCircuits.io⁶², we then identified sparsely expressing GAL4 driver lines with expression predicted to match at least one of these cells of interest. Of the 62 GAL4s identified, 17 drivers were matched to at least 3 cells each and altogether covered the majority of putative downstream cells (77%), and 11 were publicly available (Supplementary Data 2).

If *beat-la* knockdown in NPF cells increases sleep by reducing NPF input into the SEZ, then knocking down the NPF receptor (*NPFR*) in downstream cells should also increase sleep. We expressed *NPFR* RNAi using each of the candidate GAL4s and found excess sleep with two drivers, R10G06 and R16F08, that label 3 overlapping cells in the SEZ (Fig. 9B). Following this initial candidate screen, we replicated

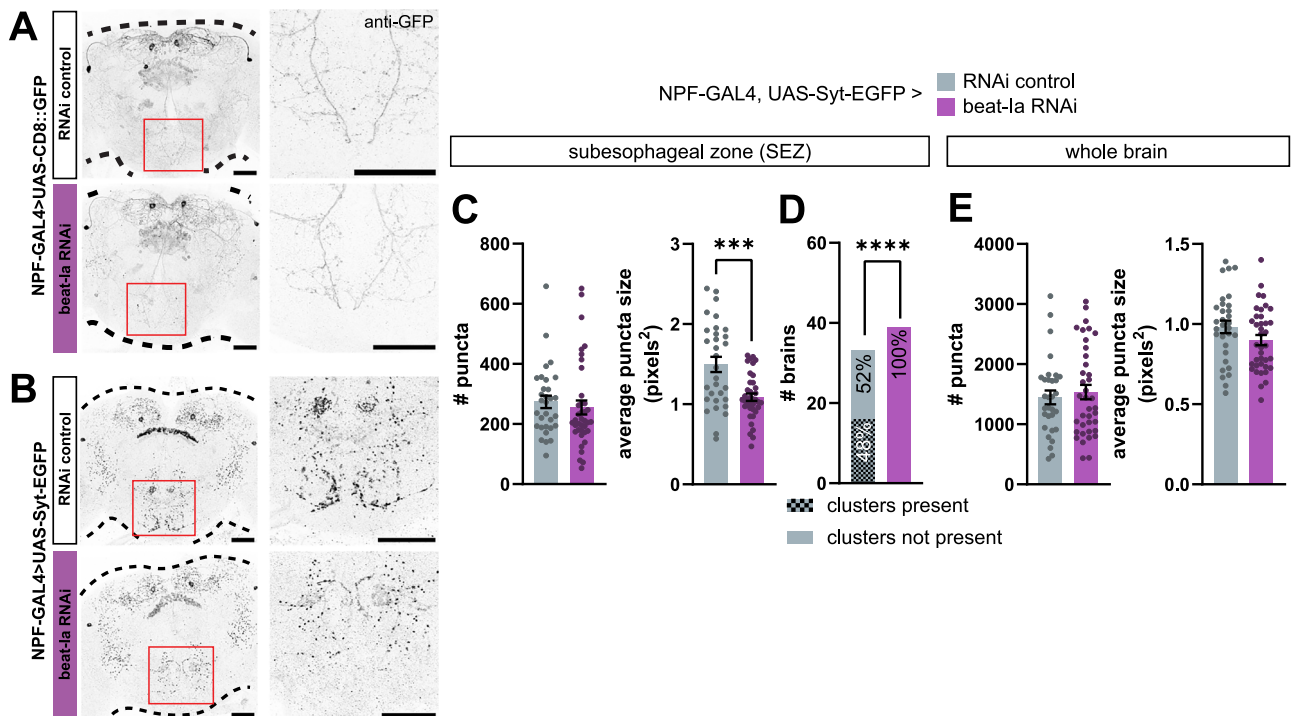


experiments and found a consistent increase in sleep with R10G06 > *NPFR* RNAi (Supplementary Fig. 16), while the phenotype with R16F08 was only significantly different compared to one parental control (Supplementary Fig. 17). *NPFR* knockdown in R10G06 cells also increased time spent in long sleep bouts (Supplementary Fig. 16K-M), demonstrating that reduced NPF signaling onto these cells increases both sleep duration and sleep depth. The NPF circuit normally

promotes or maintains arousal, so manipulating these cells downstream of NPF input would be predicted to modulate sleep. Inhibition of cells defined by R10G06 using *UAS-Kir2.1*, an inwardly rectifying potassium channel, resulted in increased sleep (Fig. 9C), similar to *NPFR* knockdown or loss of NPF input via *beat-la* RNAi (R16F08>*Kir2.1* was lethal). We then tested activation of R10G06 cells with the heat-sensitive cation channel *UAS-TrpA1* and observed a reduction in sleep

Fig. 6 | A targeted spatial knockdown screen reveals a role for *beat-1a* in neuropeptide F (NPF) cells. **A** Total sleep duration for flies expressing *beat-1a* RNAi or control in known sleep- and circadian-regulatory cell populations. Two-way ANOVA with Šidák's multiple comparisons tests comparing experimental genotypes to control. $n = 16$ except for TRH-GAL4>*beat-1a* RNAi (15), TDC2-GAL4>RNAi control (14), TDC2-GAL4>*beat-1a* RNAi (14), per-GAL4>RNAi control (10), per-GAL4>*beat-1a* RNAi (15), and pdf-GAL4>*beat-1a* RNAi (15). **B** Sleep trace. **C** Total sleep duration. **D–G** Day sleep measures. **H–K** Night sleep measures. One-way ANOVA with Šidák's multiple comparisons test comparing all genotypes. **L–N** Proportion of total, day,

and night sleep spent in long (> 60 min) vs. short (< 60 min) sleep bouts. Fisher's exact test, two-sided. n , all genotypes = 32. Spatial screen (**A**) was run with single-beam DAM monitors; all other sleep experiments were run with multibeam DAM monitors. Cell populations targeted: ChAT = cholinergic cells, TH = dopaminergic cells, TRH = serotonergic cells, Gad1 = GABAergic cells, TDC2 = octopaminergic cells, dilp = insulin-like peptide-secreting cells, Dh44 = diuretic hormone 44-producing cells, cry, per, pdf, tim = clock cells, NPF = neuropeptide F-producing cells. $**p \leq 0.01$, $***p \leq 0.001$, $****p \leq 0.0001$. Each datapoint represents one animal. Bar plots display mean \pm SEM. Source data are provided as a Source Data file.



and night sleep spent in long (> 60 min) vs. short (< 60 min) sleep bouts. Fisher's exact test, two-sided. n , all genotypes = 32. Spatial screen (**A**) was run with single-beam DAM monitors; all other sleep experiments were run with multibeam DAM monitors. Cell populations targeted: ChAT = cholinergic cells, TH = dopaminergic cells, TRH = serotonergic cells, Gad1 = GABAergic cells, TDC2 = octopaminergic cells, dilp = insulin-like peptide-secreting cells, Dh44 = diuretic hormone 44-producing cells, cry, per, pdf, tim = clock cells, NPF = neuropeptide F-producing cells. $**p \leq 0.01$, $***p \leq 0.001$, $****p \leq 0.0001$. Each datapoint represents one animal. Bar plots display mean \pm SEM. Source data are provided as a Source Data file.

(Fig. 9D, Supplementary Fig. 18), supporting a role in arousal. Further connectome analysis revealed that R10G06-GAL4 (and R16F08-GAL4) expresses in three specific candidate cells of the SEZ downstream of NPF neurons (GNG.590, GNG.743, and GNG.651), all of which are predicted by machine learning analysis of electron microscopy to be GABAergic⁶³ and project almost exclusively to other cells within the SEZ (Fig. 9E, F). Together, these data support a model in which a subpopulation of ventrally-projecting NPF cells may activate GABAergic neurons in the SEZ to maintain wakefulness, and that excessive sleep can emerge from developmental miswiring of this circuit (Supplementary Fig. 19).

NPY receptor agonism rescues long sleep phenotype in *cadm2b* crispant zebrafish

Our evidence in flies defines a developmental origin of adult hypersomnia but implicates a specific signaling system (NPF) whose dysfunction can be targeted. To avoid confounds related to oral administration of peptides in flies, we examined pharmacologic manipulation of NPY signaling in *cadm2b* crispant zebrafish, in which drugs can be bath applied⁶⁴. While *Drosophila* express only one

isoform of the NPF receptor, zebrafish express five NPY receptor subtypes⁶⁵, including an NPY Y2 isoform that is highly homologous to both human NPY Y2 and *Drosophila* NPF receptor⁶⁶. We administered a selective agonist of the human NPY Y2 receptor, Peptide YY (3-36)^{67,68}, and measured sleep in *cadm2b* crispants and sibling negative control-injected fish. As expected, without Peptide YY (PYY) administration, *cadm2b* crispants slept significantly more than controls (Fig. 9G). Remarkably, with PYY administration, excess sleep during both day and night in *cadm2b* crispants was attenuated, reaching similar sleep duration to control fish (Fig. 9G, Supplementary Fig. 20). PYY exposure in controls had no significant effects on sleep, supporting specific efficacy of the drug in the setting of hypersomnia with loss of *cadm2b* (Fig. 9G). These findings suggest conserved impairment of NPF/NPY signaling with loss of *beat-1a/cadm2b* and point towards NPY agonism as a therapeutic avenue in human hypersomnia.

Discussion

Disorders of excessive sleepiness are poorly studied, with few mechanistic insights. Leveraging a comprehensive TAD-wise analysis of putative candidate genes related to GWAS-implicated hypersomnia

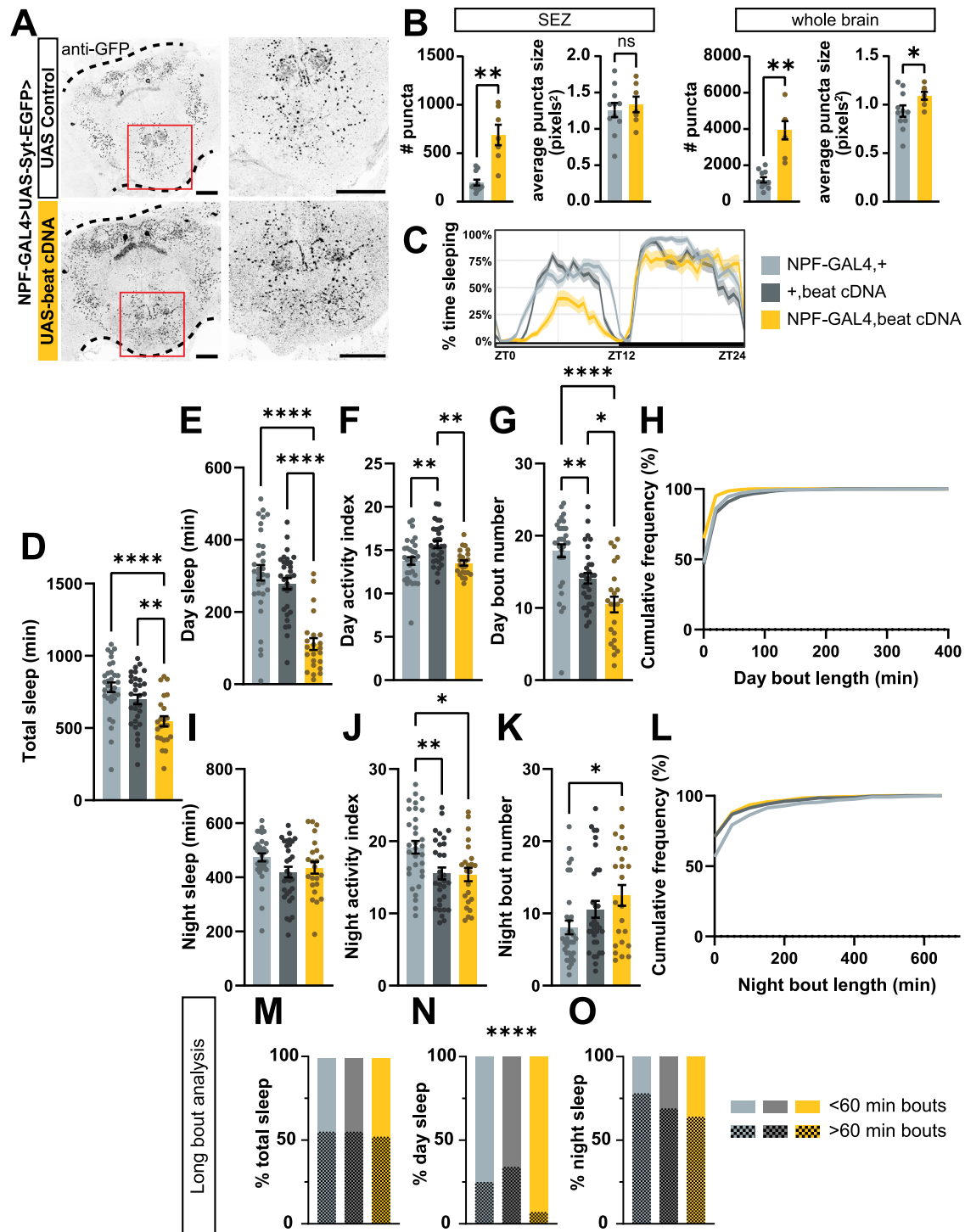
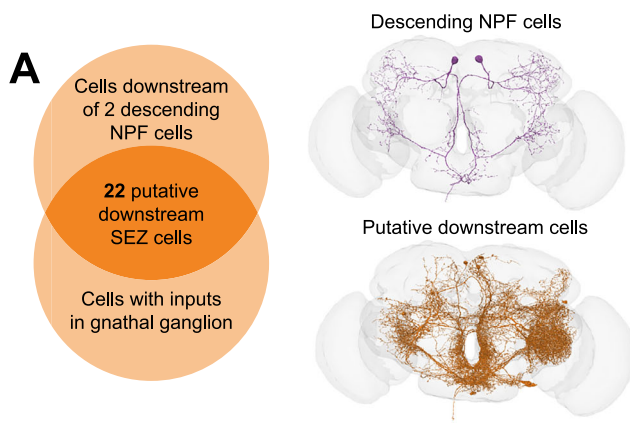


Fig. 8 | *beat-1a* overexpression in NPF cells increases synapse number and reduces sleep. **A** Representative images from flies expressing presynaptic reporter Syt-EGFP and *beat-1a* cDNA or a UAS control using the NPF-GAL4 driver. Scale bar = 50 μm. **B** Quantification of Syt-EGFP-tagged puncta across entire brain and in SEZ. Welch's t test, two-tailed. n, left to right = 11, 7. **C** Sleep trace. **D** Total sleep duration. **E-H** Day sleep measures. **I-L** Night sleep measures. One-way ANOVA with Tukey's

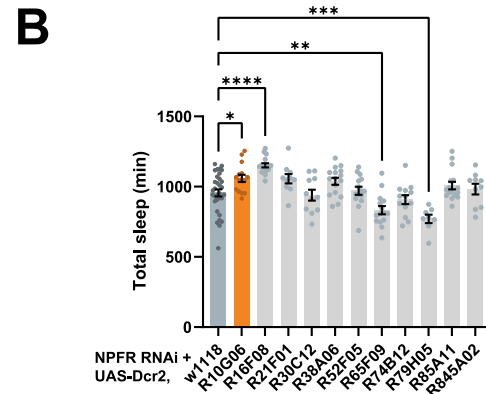
multiple comparisons tests to compare experimental genotype to controls. **M-O** Proportion of total, day, and night sleep spent in long (> 60 min) vs. short (< 60 min) sleep bouts. Fisher's exact test, two-sided. Sleep experiments were run with multibeam DAM monitors. n, from left to right = 32, 31, 23. * p ≤ 0.05, ** p ≤ 0.01, **** p ≤ 0.0001. Each datapoint represents one animal. Bar plots display mean +/- SEM. Source data are provided as a Source Data file.

loci, we describe a conserved role for synaptic adhesion molecules *beat-1a* and *CADM2* in sleep regulation. Specifically, *beat-1a* patterns sleep circuits during development, guiding wiring of NPF neurons to promote normal arousal in adulthood. Our results indicate that descending NPF projections to the SEZ may undergo synapse elaboration

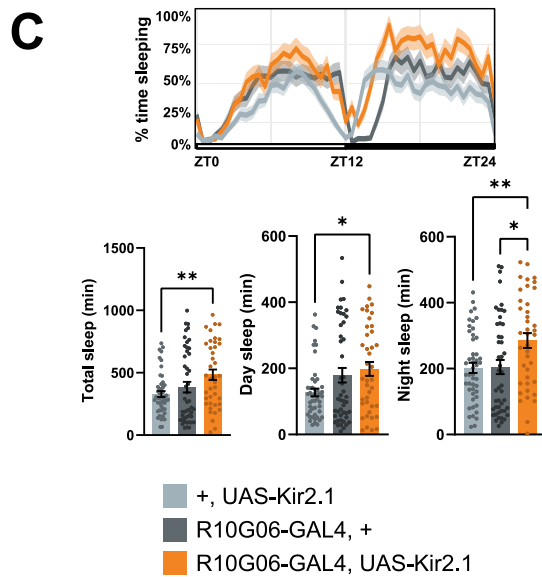
onto a small population of wake-promoting GABAergic neurons. With loss of *beat-1a*, these synapses fail to develop normally, possibly resulting in impairment of the arousal-stabilizing NPF signal and excessive sleepiness in adulthood (Supplementary Fig. 19). Pharmacologic evidence in zebrafish suggests similar NPY circuit impairment



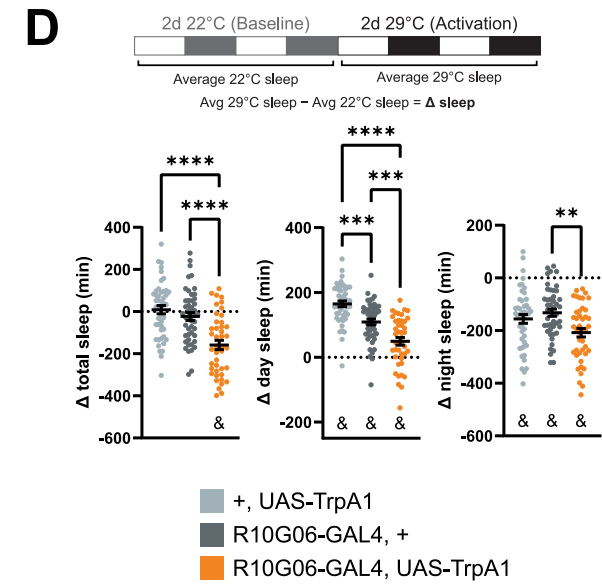
NPF Receptor Knockdown Screen



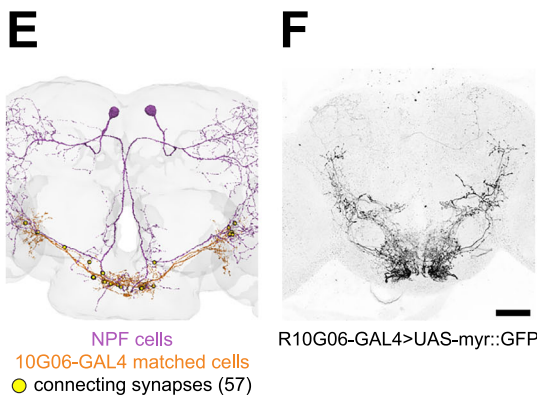
Inactivation (Kir2.1)



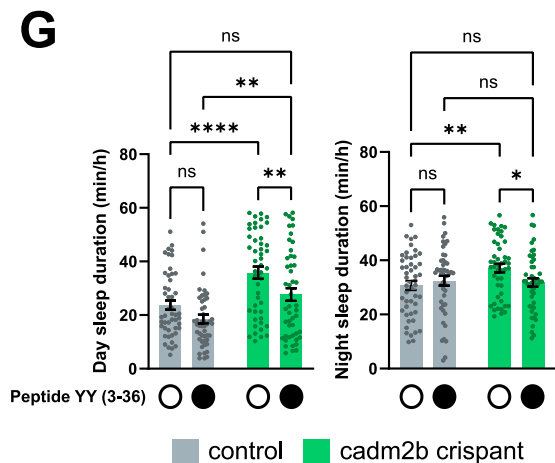
Activation (TrpA1)



Expression Pattern



NPY Receptor Agonism



with loss of *cadm2b* that can be corrected with an NPY receptor agonist. Combining human genomics with experimental observations in fish and flies, our findings uncover a previously unrecognized neurodevelopmental basis for IH stemming from dysfunction of a targetable neuropeptidergic system.

beat-1a knockdown in neuropeptide F (NPF) cells is sufficient to cause sleepiness in adult flies, putatively through loss of NPF synaptic

innervation in development and impaired NPF signaling in adulthood. NPF is the *Drosophila* homolog of vertebrate neuropeptide Y (NPY), and both NPF and NPY play a role in numerous behaviors, including feeding, social behavior, learning, circadian rhythmicity, and sleep. Both wake- and sleep-promoting roles have been described for NPF/NPY, depending on manipulation, sex, and organism. In zebrafish, global overexpression of NPY promotes sleep and loss of NPY reduces

Fig. 9 | Identification of downstream SEZ cells that regulate sleep. **A** Schematic of connectome-assisted identification of putative SEZ cells downstream of NPF. Images taken from FlyWire Connectome Codex^{60,82}. **B** Initial screen of sleep with NPF receptor knockdown in SEZ cells. *n*, left to right = 32, 15, 16, 10, 11, 16, 15, 15, 13, 8, 16, 10. **C** Sleep with inactivation of 10G06 cells using the inwardly rectifying potassium channel Kir2.1. *n*, from left to right = 40, 48, 47. **D** Sleep with activation of 10G06 cells with heat-sensitive cation channel TrpA1. Change in sleep due to activation was calculated by taking the difference of each sleep measure at 29 °C from sleep at 22 °C. *n*, left to right = 47, 46, 43. One-way ANOVA with Dunnett's multiple comparisons tests comparing experimental genotypes to controls. Sleep experiments were run with multibeam DAM monitors. **E** EM-reconstructed traces of NPF

cells and cells matched to 10G06-GAL4. Images taken from Neuroglancer⁶⁰. **F** Expression pattern in adult brain of 10G06-GAL4. Scale bar = 50 μm. **G** Day and night sleep duration in negative control siblings and *cadm2b* crispant zebrafish with or without NPY Y2 receptor agonism by Peptide YY (3-36). Two-way ANOVA with Uncorrected Fisher's LSD comparing within genotypes no drug to Peptide YY, within drug conditions negative control siblings to *cadm2b* crispants, and negative control siblings with no drug to *cadm2b* crispant on Peptide YY. *n* = 48 for all genotypes. * $p \leq 0.05$, ** $p \leq 0.01$, *** $p \leq 0.001$, **** $p \leq 0.0001$. Each datapoint represents one animal. Bar plots display mean \pm SEM. Source data are provided as a Source Data file.

sleep⁶⁹. In *Drosophila*, activation of specific NPF subpopulations promotes wakefulness⁵², while others might be sleep-promoting⁵¹. Our findings, combined with previous results, support the hypothesis that such varied effects are likely due to NPF's diverse downstream targets; *NPFR* is expressed widely across the brain⁵², and NPFR activation could result in inhibition or excitation of either wake- or sleep-promoting cells depending on the circuit. While pharmacologic results support NPY dysfunction with loss of *cadm2b* in zebrafish, future work will aim to define how specific NPY microcircuits are affected, as parsing sleep-versus arousal-promoting roles, among other behaviors like feeding, will clarify NPY-related mechanisms of excessive sleepiness across phylogeny.

Our work also reveals that *beat-la* and its receptor *side* have a role in neurodevelopment in the central brain. Until now, *beaten path* signaling has only been implicated in motor neuron^{31,34} and visual system development^{70,71}, but here we demonstrate a role for *beat-side* signaling in the development of central brain circuits, including but not limited to NPF cells. We focused specifically on *beat-la* but knockdown of several other *beat* isoforms also produced sleep phenotypes. It is possible that *beats* and *sides* act in a combinatorial manner to pattern numerous central brain circuits, as they have been predicted to act in other neural tissues⁷².

By intersecting our experimental findings with the FlyWire *Drosophila* whole-brain connectome, we identified three GABAergic neurons in the SEZ downstream of NPF cells that may be part of a sleep-regulatory circuit. Knockdown of *NPFR* and/or inhibition of these cells defined by the R10G06-GAL4 driver promoted sleep, and activation promoted arousal. NPF cells likely signal onto GABAergic SEZ cells, activating these neurons which then inhibit downstream, sleep-promoting targets, resulting in wakefulness (ON \rightarrow ON \rightarrow OFF \rightarrow wake). In *beat-la* knockdown animals, we predict that NPF cells do not signal onto SEZ GABAergic cells, thus disinhibiting downstream sleep-promoting neurons and allowing excess sleep to occur (OFF \rightarrow OFF \rightarrow ON \rightarrow sleep) (Supplementary Fig. 19). Such circuit organization is broadly similar to that of GABAergic cells in the mouse lateral hypothalamus, which inhibit sleep-promoting neurons in the ventrolateral preoptic area during wakefulness and are inactive during sleep⁷³. This model supports the hypothesis that some forms of IH result from impaired stability of arousal, and pinpoints specific neuropeptide signaling systems at play.

Finally, our work highlights a role for immunoglobulin synaptic adhesion molecules such as *beat-la* and *CADM2* in sleep regulation. In mammals, Ig containing neural cell adhesion molecules (NCAMs), similar to *CADM2*, have been found to act in adulthood to regulate sleep and circadian function^{35,74}, but specific mechanisms have remained elusive and developmental roles have not been described. Neurodevelopmental disorders with links to synaptic adhesion molecule alterations^{33,75} are commonly comorbid with sleep disturbances^{76,77}, suggesting a shared etiology. Our findings demonstrate that some sleep disorders themselves, including hypersomnias, could stem from neurodevelopmental disturbances yet remain correctable in adulthood.

Limitations of the study

Although our findings demonstrate a role for *beat-la* in NPF cells, it is possible that *beat-la* also acts in other neuronal populations to regulate sleep. Notably, knockdown of *beat-la* in cholinergic cells using cha-GAL4 significantly increased sleep. We focused on the sleep phenotype observed with NPF-GAL4 due to the driver's relatively sparse expression pattern; cha-GAL4 labels a broad population of cells, presenting a challenge for conducting further morphological or functional investigation. Additionally, while our findings implicate miswiring of NPF projections to the SEZ, other aspects of NPF circuitry could contribute to the sleep phenotype observed with loss of *beat-la* as well. For example, our manipulation of R10G06-GAL4-defined cells produced less extreme sleep phenotypes than that of *beat-la* manipulations, raising the possibility that these cells represent only part of the downstream sleep-regulatory circuit.

Methods

Drosophila husbandry

Unless otherwise specified, flies were raised and maintained on standard molasses food (8.0% molasses, 0.55% agar, 0.2% Tegosept, and 0.5% propionic acid) at 25 °C on a 12 h:12 h light:dark (LD) cycle. For experiments co-expressing *beat-la* RNAi with another UAS, animals were raised at 29 °C to prevent loss of RNAi efficacy due to GAL4 dilution. UAS-mCherry (BDSC #35787) or UAS-Luciferase (BDSC 35788) from the TRiP RNAi control fly stocks were used as controls for TRiP RNAi: UAS-mCherry was used for Figs. 1, 2, 4D-E, 5, 6A, S1, S4, S5, S10, and UAS-Luciferase was used for Figs. 3, 4A-C, 6B-N, 7, 8, S2, S3, S5, S7, S9, S11, S12, S13, S15, S16, S17. 5-7 d old female flies were used in all experiments unless otherwise noted.

Drosophila strains

Genotype	Source	Identifiers, Notes
UAS- <i>beat-la</i> RNAi (1)	BDSC	BDSC #54820; TRiP HMJ21539
UAS- <i>beat-la</i> RNAi (2)	BDSC	BDSC #64938; TRiP HMC05811
UAS-Luciferase (RNAi control)	BDSC	BDSC #35788
UAS-mCherry (RNAi control)	BDSC	BDSC #35787
UAS- <i>side-I</i> RNAi	BDSC	BDSC 50642; TRiP HMC03042
elav-GAL4	Lab stocks	outcrossed to iso31
UAS-Dcr2	Lab stocks	outcrossed to iso31
OK6-GAL4	BDSC	BDSC #64199
OK371-GAL4	BDSC	BDSC #26160

D42-GAL4	BDSC	BDSC #8816
tubGAL80ts	Lab stocks	outcrossed to iso31
ChAT-GAL4	BDSC	BDSC #6798
TH-GAL4	Lab stocks	
Gad1-GAL4	BDSC	BDSC #51630
TDC2-GAL4	Lab stocks	
dilp-GAL4	Lab stocks	
Dh44-GAL4	Lab stocks	
cry-GAL4	Lab stocks	
per-GAL4	Lab stocks	
pdf-GAL4	Lab stocks	
tim-GAL4	Lab stocks	
NPF-GAL4	BDSC	BDSC #25681, outcrossed to iso31
UAS-CD8::GFP	Lab stocks	
UAS-Syt-EGFP	Lab stocks	
UAS-Syt-EGFP	BDSC	BDSC #6926
UAS-beat-1a cDNA	Hermann Aberle	outcrossed to iso31
iso31	Lab stocks	wild-type
UAS-NPFR RNAi	VDRC	VDRC #107663
UAS-Kir2.1	Lab stocks	outcrossed to iso31
UAS-TrpA1	Lab stocks	outcrossed to iso31
w1118	Janelia Research Campus	wild-type
VDRC RNAi control;	VDRC	VDRC #60100; KK RNAi library control
UAS-SoxN RNAi	BDSC	BDSC #64930; TRiP HMC05803
ChA-GAL80	Lab stocks	
nsyb-GeneSwitch	Lab stocks	outcrossed to iso31
R23E10-GAL4	BDSC	BDSC #49032
SS01587	BDSC	BDSC #75917

Gene identification, TAD analysis

TAD boundaries were downloaded from <http://3dgenome.fsm.northwestern.edu/>⁷⁸ for hg19 HI-NPCs²² to determine the extent of the TAD encompassing rs1601440. Locus zoom plots were created using the Sleep Disorders Knowledge Portal (<https://sleep.hugeamp.org/>) with the LD reference SNP set at rs1601440 for against the EUR reference panel.

Sleep assays

Adult female flies were collected 2–3 d after eclosion and aged to 5–7 d in group housing at 25 °C on a 12 h:12 h light:dark schedule, unless otherwise noted. Female flies were housed with males to ensure mated status upon loading. Flies were then anesthetized on CO₂ pads (Genesee Scientific, #59-114) and loaded into individual glass tubes supplied with 5% sucrose, 2% agar food. Tubes were then loaded into Drosophila Activity Monitoring systems (Trikinetics) and flies were monitored for at least 2 d. Activity was measured in 1 min bins and sleep was defined as 5 min of inactivity, except for long bout analyses for which sleep was defined as 60 min of inactivity. Activity indices were measured as number of beam breaks per 1 m of waking activity. Data was analyzed using Rethomics.

Sleep deprivation

Following baseline day sleep measurement from ZT0-12, flies received a 2 s stimulation randomly within every 20 s window from ZT12-ZT24 using a mechanical vortexer (Fisher Multitube Vortexer, Catalog # 02-215-450).

Arousal threshold

The Universal Vibration Stage (UVS-01, Tau Scientific) was used to deliver 1 s, 20 hz, 0.4 volume stimuli once per hour from ZT1 to ZT24 totaling 24 timepoints per animal. Flies were defined “aroused” if they were in a > 5 m immobility bout prior to stimulation and made a beam break within 2 m after stimulation, and “not aroused” if they were in a > 5 m immobility bout that was not broken by stimulation. “Arousability” was measured per fly as # times aroused/# of times not aroused.

Sleep latency

Adult female flies were loaded into the single beam DAM system as previously described. Sleep latency was measured by identifying animals that were woken by the light transition at ZT0 and measuring time lapsed until their next sleep bout, averaging sleep latency across two days. Animals that were awake at the time of the light transition or who were not woken were excluded.

Circadian rhythmicity analysis

Flies were loaded into the DAM system 5–7 d after eclosion and entrained to a 12 h:12 h LD cycle for 4 d before transferred to constant darkness (DD). Locomotor activity was measured for 11 d in DD. Locomotor rhythmicity was analyzed by Fast Fourier transform (FFT) using ClockLab software (Actimetrics, Wilmette, IL), and the maximum FFT amplitude was calculated to determine rhythmicity: rhythmic (FFT ≥ 0.05), moderately rhythmic (0.05 > FFT ≥ 0.03), weakly rhythmic (0.03 > FFT ≥ 0.01), or arrhythmic (< 0.01). Period length was calculated only from flies that were not categorized as arrhythmic.

Temporal mapping experiments

Temperature-dependent RNAi expression (tubGAL80ts). Using elav-GAL4; tubGAL80ts to drive RNAi, flies were held at 18 °C to permit GAL80 expression and block RNAi expression or were held at 29 °C to denature GAL80 and allow gene knockdown. The following temperature shift schedules were used to restrict knockdown to developmental stages:

For pre-eclosion knockdown, parental crosses were raised at 29 °C and immediately upon eclosion progeny were collected and moved to 18 °C. Progeny were aged to 5–7 d and sleep assays were conducted at 18 °C.

For post-eclosion knockdown, parental crosses were raised at 18 °C and immediately upon eclosion progeny were collected and moved to 29 °C. Progeny were aged to 5–7 d and sleep assays were conducted at 29 °C.

For pupal knockdown, parental crosses were raised at 18 °C until wandering third instar larvae were observed, at which point crosses were moved to 29 °C. Immediately upon eclosion, progeny were collected and moved to 18 °C. Progeny were aged 5–7 d and sleep assays were conducted at 22 °C.

Hormonally induced RNAi expression (nsyb-GeneSwitch). 50 mM RU486 stock solution was prepared by dissolving RU486 (Thermo Fisher Scientific) in 100% ethanol (EtOH), which was then diluted in either standard molasses food or sucrose agar to make 200 μM working solution. An equal volume of 100% EtOH was used as a vehicle control. Animals were fed RU486 or EtOH starting at 4 d post-pupation and sleep data collection began at 6 d post-pupation.

Generation of zebrafish mutant

Zebrafish experiments were performed in accordance with the University of Pennsylvania Institutional Animal Care and Use Committee guidelines.

Wild-type (AB/TL) embryos were collected in embryonic growth media (E3 medium; 5 mM NaCl, 0.17 mM KCl, 0.33 mM CaCl₂, 0.33 mM MgSO₄) in the morning shortly after lights-on. Pre-formed ribonuclear protein complexes containing the guide RNAs (gRNA) and Cas9 enzyme were injected at the single-cell stage. Negative control sequences are: 5'-CGTTAATCGCGTATAATACG-3' and 5'-CAT-ATTGCGCGTATAGTCGC-3'. For *cadm2b*, two gRNAs were designed using the online tool Crispor (<http://crispor.tefor.net/>) with the reference genome set to "NCBI GRCz11" and the protospacer adjacent motif (PAM) set to "20bp-NGG-Sp Cas9, SpCas9-HF, eSpCas9 1.1." gRNAs were prioritized by specificity score (>95%) with 0 predicted off-targets with up to 3 mismatches. The zebrafish sequence was obtained using Ensembl (<https://useast.ensembl.org/>) with GRCz11 as the reference genome. Sequence was aligned to the human amino acid sequence using MARRVEL to identify the coding region with highest conservation, and each gRNA was designed targeting conserved exonic regions. gRNA 1 was designed to target exon 3 of transcript 201 with the guide sequence 5'-TTGAAGTGGTCCGAGCCTCG-PAM-TGG-3'; Left primer 5'-TCAGCATTGAGGGACAACCG-3'; Right primer 5'-ATGACTGGGAGAGAACGCAC-3'; Headloop sense primer 5'-CGAGGCTCGGACCAGTTCATCAGCATTGAGGGACAACCG-3'. gRNA 2 was designed to target exon 4 of transcript 201 with the guide sequence (reverse strand) 3'-CCG-PAM-ATGGTTCAGGAACGACAAGG-5'; Left primer 5'-TCCTGCTGCTCTGTTGTGT-3'; right primer 5'-ACACAGATCACGCACCACTT-3' and restriction enzyme BclI. DNA extraction was performed per the manufacturer's protocol (Quanta bio, Beverly, MA) immediately following completion of the sleep assay (8 days post fertilization), as described previously^{8,48}. Genotyping was performed on individual fish at the conclusion of each sleep assay by PCR following manufacturer's protocols (64° for Headloop PCR using Phusion HF DNA polymerase and 60° for restriction digest using GoTaq Green Master Mix). Mutation efficiency was quantified by band intensity as the ratio of headloop primer: standard primer and cut:uncut, and fish were included in behavioral analysis provided they show >90% efficiency in at least 1 guide RNA as described previously⁴⁸. All primers were run on a 2% agarose gel and sequence verified using Sanger sequencing to verify the target region.

Data collection and analysis for sleep phenotyping in zebrafish

On day 5 post fertilization, CRISPR mutants and scramble-injected sibling controls were pipetted into individual wells of a 96-well plate and placed into a Zebrafish box (Viewpoint Life Sciences) for automated video monitoring. Genotypes were placed into alternating rows to minimize location bias within the plate. Each zebrafish box is sound-attenuating and contains circulating water held at a temperature of 28.5 °C with automated lights cycling on the same 14 h:10 h light/dark cycle. E3 media was topped off at lights-on (9am) every day. Sleep-wake behaviors were measured through automated video-tracking, as described previously^{8,48,64}.

Activity data were captured using automated video tracking (Viewpoint Life Sciences) software in quantization mode. As described previously⁷⁹, threshold for detection was set as the following: detection threshold: 20; burst: 29; freeze: 3; bin size: 60 s. Data were processed using custom MATLAB scripts⁸⁰ with the threshold for sleep set at 1 min with <0.5 s of activity. All animals were allowed to acclimate to the zebrafish box for approximately 24 h before beginning continuous data collection for 48 h starting at lights-on. Two biological replicates were performed swapping row order in the plate. Data were visually inspected to exclude extreme outliers indicating technical artifact or abnormal development/death.

Peptide YY (3-36) administration and sleep phenotyping

Peptide YY (3-36) (PYY) was obtained from Tocris (#1618) and dissolved in water to achieve a 100 μM stock solution. Fish were allowed to develop and hatch normally without manual dechoriation. On day 3 post fertilization, larvae were placed into individual wells of a 96-well plate and E3 media was filled to be flush with the top of each well (650 μl). PYY was dissolved in water and 0.65 μl was administered directly to the well at a concentration of 50 μM to give a final drug concentration of 50 nM in each well. An equal volume of water was added to negative control wells. PYY was administered at 2 pm on days 3 and 4 post fertilization when E3 was topped off in each well. Fish were allowed to acclimate to the box and sleep was measured as described above except sleep-wake behaviors were only measured on day 4 to capture acute effects of drug administration. Two biological replicates were performed swapping row order in the plate.

CAFÉ assay

Feeding was measured using a modified version of the Capillary Feeder assay. 10 adult female flies were transferred from normal food vials to agar-only vials. Affixed to the vials was a rubber stopper with one glass pipet (World Precision Instruments, #1B150F-4), initially empty. Animals were starved in this chamber overnight, also allowing for habituation to the glass pipet. At ZT1, the empty glass pipet was replaced with a pipet filled with 2% sucrose solution, dyed blue (FD&C Blue #1, Fisher #S06652) and topped with a drop of mineral oil to prevent evaporation. Meniscus movement was measured over 6 h. Both the habituation and experimental periods were conducted in a 25 °C humidity-controlled incubator.

Starvation resistance assay

Flies were loaded into the single beam DAM system as previously described for sleep assays, except DAM tubes were filled with 2% agar-only food. Data was collected until all animals were deceased, roughly 4 days.

qPCR

20 female adult brains per sample were dissected on 1X phosphate-buffered saline, with 3 biological replicates per genotype. RNA was then extracted using the RNeasy Plus Mini Kit (Qiagen, #74136). Primers were designed against *beat-la A* and *B* isoforms, and neuronal tubulin was used as a housekeeping gene. RNA was amplified using SsoAdvanced SYBR Green Supermix and amplification was measured using a CFX Opus 96 Real-Time PCR System. Relative changes in *beat* mRNA expression were quantified using the 2^{-ΔΔCt} method.

Primers against *beat-la AB*

Forward: GTCCTCGAACGAGAGCCAAG

Reverse: GCATTGTGGGGCGTTCAATAA

Immunohistochemistry

Fly brains were dissected in 1X phosphate-buffered saline (PBS) and fixed in 4% paraformaldehyde (PFA) for 15 min at room temperature. Samples were then washed three times for 15 min each in PBS with 0.1% Triton X-100 (PBST) and then blocked in PBST with 5% goat serum for 1 h at room temperature. Samples were then incubated with primary antibody in PBST with 5% goat serum at 4 °C overnight. Samples were then washed three times for 15 min each in PBST and incubated with secondary antibody in PBST with 5% goat serum at 4 °C overnight. Samples were then washed three times for 15 min each in PBST, cleared in 50% glycerol, and mounted in VECTASHIELD. The following primary antibodies were used: rabbit anti-GFP (1:500, Invitrogen, CAT # A11122), mouse anti-GFP (1:500, Fisher, CAT # G6539), rabbit anti-NPF⁸¹ (1:250, RayBioTech, CAT # RB-19-0001-20), mouse anti-nc82 (1:100, DSHB, CAT # nc82). The following secondary antibodies were used (all at 1:250, ThermoFisher): goat anti-mouse 488 (CAT # A32723), donkey

anti-mouse 594 (CAT # A32744), goat anti-rabbit 488 (CAT # A32731TR), and goat anti-rabbit 594 (CAT # A32740).

Imaging and analysis

Microscopy images were taken using a Leica TCS SP8 confocal microscope. Unless otherwise specified, maximum projection images were generated of all Z-slices, with images taken in 0.5 μ M steps. If necessary for whole-brain visualization, images were stitched using GIMP. All other image analysis was conducted in ImageJ.

Syt-EGFP puncta analysis. Maximum projection images of Syt-EGFP samples were generated. Cell bodies were selected and deleted to avoid quantification of extraneous non-synaptic signal. Additionally, the fan body was selected and deleted to ensure accurate puncta size measurements, as Syt-EGFP signal is not punctated in the fan body and more detailed analyses on the fan body were performed separately. ROIs of the entire sample and of the SEZ were defined, using nc82 as an anatomical stain. The EGFP channel was isolated from the merged image and converted to a binary image using ImageJ's Intermodes dark no-reset threshold. The Analyze Particles function was then used to count and measure all objects larger than 1.50 pixels².

Syt-EGFP dorsal fan-shaped body quantification. Z-stacks of Syt-EGFP samples were cropped to only slices containing the fan body and sum projection images were generated. An ROI of the fan body was defined using nc82 as an anatomical stain. The EGFP channel was isolated from the merged image and GFP fluorescence was quantified.

Statistical analysis

All statistical analyses were performed using GraphPad Prism. Details on sample sizes and statistical tests are denoted in figure legends. For all figures, * $p \leq 0.05$, ** $p \leq 0.01$, *** $p \leq 0.001$, **** $p \leq 0.0001$, and bar plots display mean \pm SEM unless otherwise specified.

Data availability

All data needed to evaluate the conclusions in the paper are present in Source Data and/or Supplementary Data files. Source data are provided with this paper.

References

- Grandner, M. A. Sleep, health, and society. *Sleep. Med. Clin.* **15**, 319–340 (2020).
- Zamore, Z. & Veasey, S. C. Neural consequences of chronic sleep disruption. *Trends Neurosci.* **45**, 678–691 (2022).
- Lane, J. M. et al. Genetics of circadian rhythms and sleep in human health and disease. *Nat. Rev. Genet.* **24**, 4–20 (2023).
- Sehgal, A. & Mignot, E. Genetics of Sleep and Sleep Disorders. *Cell* **146**, 194–207 (2011).
- Chakravarti, L., Moscato, E. H. & Kayser, M. S. Unraveling the Neurobiology of Sleep and Sleep Disorders Using Drosophila. in *Current Topics in Developmental Biology* vol. 121 253–285 (Elsevier, 2017).
- Donelson, N. C. & Sanyal, S. Use of Drosophila in the investigation of sleep disorders. *Exp. Neurol.* **274**, 72–79 (2015).
- Raizen, D., Mason, T. & Pack, A. Genetic basis for sleep regulation and sleep disorders. *Semin Neurol.* **26**, 467–483 (2006).
- Palermo, J. et al. Variant-to-gene mapping followed by cross-species genetic screening identifies GPI-anchor biosynthesis as a regulator of sleep. *Sci. Adv.* **9**, eabq0844 (2023).
- Gottlieb, D. J., O'Connor, G. T. & Wilk, J. B. Genome-wide association of sleep and circadian phenotypes. *BMC Med. Genet.* **8**, S9 (2007).
- Raizen, D. M. & Wu, M. N. Genome-wide association studies of sleep disorders. *Chest* **139**, 446–452 (2011).
- Trotti, L. M. Idiopathic hypersomnia. *Sleep. Med. Clin.* **12**, 331–344 (2017).
- Trotti, L. M. & Arnulf, I. Idiopathic hypersomnia and other hypersomnia syndromes. *Neurotherapeutics* **18**, 20–31 (2021).
- Arnulf, I., Leu-Semenescu, S. & Dodet, P. Precision medicine for idiopathic hypersomnia. *Sleep. Med. Clin.* **17**, 379–398 (2022).
- Sforza, E., Hupin, D. & Roche, F. Mononucleosis: a possible cause of idiopathic hypersomnia. *Front. Neurol.* **9**, 922 (2018).
- Landzberg, D. & Trotti, L. M. Is idiopathic hypersomnia a circadian rhythm disorder? *Curr. Sleep Med. Rep.* <https://doi.org/10.1007/s40675-019-00154-x>. (2019).
- Materna, L. et al. Idiopathic hypersomnia patients revealed longer circadian period length in peripheral skin fibroblasts. *Front. Neurol.* **9**, 424 (2018).
- Rye, D. B. et al. Modulation of vigilance in the primary hypersomnias by endogenous enhancement of GABAA receptors. *Sci. Transl. Med.* **4**, 161 151–161 151 (2012).
- Ali, M., Auger, R. R., Slocumb, N. L. & Morgenthaler, T. I. Idiopathic hypersomnia: clinical features and response to treatment. *J. Clin. Sleep. Med.* **5**, 562–568 (2009).
- Bassetti, C. & Aldrich, M. S. Idiopathic hypersomnia. A series of 42 patients. *Brain* **120**, 1423–1435 (1997).
- Anderson, K. N., Pilsworth, S., Sharples, L. D., Smith, I. E. & Shneerson, J. M. Idiopathic hypersomnia: a study of 77 cases. *Sleep* **30**, 1274–1281 (2007).
- Smemo, S. et al. Obesity-associated variants within FTO form long-range functional connections with IRX3. *Nature* **507**, 371–375 (2014).
- Dixon, J. R. et al. Topological domains in mammalian genomes identified by analysis of chromatin interactions. *Nature* **485**, 376–380 (2012).
- Beagan, J. A. & Phillips-Cremins, J. E. On the existence and functionality of topologically associating domains. *Nat. Genet.* **52**, 8–16 (2020).
- Cubeñas-Potts, C. & Corces, V. G. Topologically associating domains: an invariant framework or a dynamic scaffold? *Nucleus* **6**, 430–434 (2015).
- Way, G. P., Youngstrom, D. W., Hankenson, K. D., Greene, C. S. & Grant, S. F. Implicating candidate genes at GWAS signals by leveraging topologically associating domains. *Eur. J. Hum. Genet.* **25**, 1286–1289 (2017).
- Wang, H. et al. Genome-wide association analysis of self-reported daytime sleepiness identifies 42 loci that suggest biological subtypes. *Nat. Commun.* **10**, 3503 (2019).
- Dashti, H. S. et al. Genetic determinants of daytime napping and effects on cardiometabolic health. *Nat. Commun.* **12**, 900 (2021).
- Dashti, H. S. et al. Genome-wide association study identifies genetic loci for self-reported habitual sleep duration supported by accelerometer-derived estimates. *Nat. Commun.* **10**, 1100 (2019).
- Tanida, K. et al. Genome-wide association study of idiopathic hypersomnia in a Japanese population. *Sleep Biol. Rhythms* <https://doi.org/10.1007/s41105-021-00349-2>. (2021).
- Hu, Y. et al. An integrative approach to ortholog prediction for disease-focused and other functional studies. *BMC Bioinforma.* **12**, 357 (2011).
- Bazan, J. F. & Goodman, C. S. Modular structure of the Drosophila Beat protein. *Curr. Biol.* **7**, R338–R339 (1997).
- Pietri, T., Easley-Neal, C., Wilson, C. & Washbourne, P. Six cadm/synCAM genes are expressed in the nervous system of developing zebrafish. *Dev. Dyn.* **237**, 233–246 (2008).
- Frei, J. A. & Stoeckli, E. T. SynCAMs—from axon guidance to neurodevelopmental disorders. *Mol. Cell. Neurosci.* **81**, 41–48 (2017).
- Fambrough, D. & Goodman, C. S. The Drosophila beaten path gene encodes a novel secreted protein that regulates defasciculation at motor axon choice points. *Cell* **87**, 1049–1058 (1996).
- Cooper, J. M., Halter, K. A. & Prosser, R. A. Circadian rhythm and sleep-wake systems share the dynamic extracellular synaptic milieu. *Neurobiol. Sleep. Circadian Rhythms* **5**, 15–36 (2018).

36. Li, H. et al. Deconstruction of the beaten Path-Sidestep interaction network provides insights into neuromuscular system development. *eLife* **6**, e28111 (2017).
37. Siebert, M., Banovic, D., Goellner, B. & Aberle, H. Drosophila motor axons recognize and follow a sidestep-labeled substrate pathway to reach their target fields. *Genes Dev.* **23**, 1052–1062 (2009).
38. Jong, S., Cavallo, J. A., Rios, C. D., Dworak, H. A. & Sink, H. Target recognition and synaptogenesis by motor axons: responses to the sidestep protein. *Int. J. dev. neurosci.* **23**, 397–410 (2005).
39. Girard, F. et al. Chromatin immunoprecipitation reveals a novel role for the Drosophila Soxneuro transcription factor in axonal patterning. *Dev. Biol.* **299**, 530–542 (2006).
40. Wiggin, T. D. et al. Covert sleep-related biological processes are revealed by probabilistic analysis in *Drosophila*. *Proc. Natl. Acad. Sci. USA* **117**, 10024–10034 (2020).
41. Chowdhury, B., Abhilash, L., Ortega, A., Liu, S. & Shafer, O. Homeostatic control of deep sleep and molecular correlates of sleep pressure in *Drosophila*. *eLife* **12**, e91355 (2023).
42. Niederkofler, V., Baeriswyl, T., Ott, R. & Stoeckli, E. T. Nectin-like molecules/SynCAMs are required for post-crossing commissural axon guidance. *Development* **137**, 427–435 (2010).
43. Pellissier, F., Gerber, A., Bauer, C., Ballivet, M. & Ossipow, V. The adhesion molecule Necl-3/SynCAM-2 localizes to myelinated axons, binds to oligodendrocytes and promotes cell adhesion. *BMC Neurosci.* **8**, 90 (2007).
44. Leung, L. C. et al. Neural signatures of sleep in zebrafish. *Nature* **571**, 198–204 (2019).
45. Zhdanova, I. V. Sleep in zebrafish. *Zebrafish* **3**, 215–226 (2006).
46. Zhdanova, I. V., Wang, S. Y., Leclair, O. U. & Danilova, N. P. Melatonin promotes sleep-like state in zebrafish. *Brain Res.* **903**, 263–268 (2001).
47. Yokogawa, T. et al. Characterization of Sleep in Zebrafish and Insomnia in Hypocretin Receptor Mutants. *PLoS Biol.* **5**, e277 (2007).
48. Kroll, F. et al. A simple and effective FO knockout method for rapid screening of behaviour and other complex phenotypes. *eLife* **10**, e59683 (2021).
49. Aberle, H. Searching for guidance cues: follow the Sidestep trail. *Fly* **3**, 270–273 (2009).
50. McGuire, S. E., Mao, Z. & Davis, R. L. Spatiotemporal gene expression targeting with the TARGET and gene-switch systems in *Drosophila*. *Sci. Sig.* 2004, pl6–pl6, (2004).
51. He, C., Yang, Y., Zhang, M., Price, J. L. & Zhao, Z. Regulation of sleep by neuropeptide Y-like system in *Drosophila melanogaster*. *PLoS ONE* **8**, e74237 (2013).
52. Chung, B. Y. et al. *Drosophila* neuropeptide F signaling independently regulates feeding and sleep-wake behavior. *Cell Rep.* **19**, 2441–2450 (2017).
53. He, C. et al. Regulation of circadian locomotor rhythm by neuropeptide Y-like system in *Drosophila melanogaster*. *Insect Mol. Biol.* **22**, 376–388 (2013).
54. Ja, W. W. et al. Prandiology of *Drosophila* and the CAFE assay. *Proc. Natl. Acad. Sci. USA* **104**, 8253–8256 (2007).
55. Liu, Q., Liu, S., Kodama, L., Driscoll, M. R. & Wu, M. N. Two dopaminergic neurons signal to the dorsal fan-shaped body to promote wakefulness in *Drosophila*. *Curr. Biol.* **22**, 2114–2123 (2012).
56. Pimentel, D. et al. Operation of a homeostatic sleep switch. *Nature* **536**, 333–337 (2016).
57. Donlea, J. M., Thimgan, M. S., Suzuki, Y., Gottschalk, L. & Shaw, P. J. Inducing sleep by remote control facilitates memory consolidation in *Drosophila*. *Science* **332**, 1571–1576 (2011).
58. Donlea, J. M. et al. Recurrent circuitry for balancing sleep need and sleep. *Neuron* **97**, 378–389.e4 (2018).
59. Donlea, J. M., Pimentel, D. & Miesenböck, G. Neuronal machinery of sleep homeostasis in *Drosophila*. *Neuron* **81**, 860–872 (2014).
60. Dorkenwald, S. et al. FlyWire: online community for whole-brain connectomics. *Nat. Methods* **19**, 119–128 (2022).
61. Schlegel, P. et al. Whole-brain annotation and multi-connectome cell typing of *Drosophila*. *Nature* **634**, 139–152 (2024).
62. BrainCircuits.io. <https://braincircuits.io/> (2023).
63. Eckstein, N. et al. Neurotransmitter classification from electron microscopy images at synaptic sites in *Drosophila melanogaster*. *Cell* **187**, 2574–2594.e23 (2024).
64. Rihel, J. et al. Zebrafish behavioral profiling links drugs to biological targets and rest/wake regulation. *Science* **327**, 348–351 (2010).
65. Larhammar, D. & Salaneck, E. Molecular evolution of NPY receptor subtypes. *Neuropeptides* **38**, 141–151 (2004).
66. Garczyski, S. F., Brown, M. R., Shen, P., Murray, T. F. & Crim, J. W. Characterization of a functional neuropeptide F receptor from *Drosophila melanogaster*. *Peptides* **23**, 773–780 (2002).
67. Park, C. et al. Structural basis of neuropeptide Y signaling through Y1 receptor. *Nat. Commun.* **13**, 853 (2022).
68. Grandt, D. et al. Novel generation of hormone receptor specificity by amino terminal processing of peptide YY. *Biochem. Biophys. Res. Commun.* **186**, 1299–1306 (1992).
69. Singh, C., Rihel, J. & Prober, D. A. Neuropeptide Y regulates sleep by modulating noradrenergic signaling. *Curr. Biol.* **27**, 3796–3811.e5 (2017).
70. Carrier, Y. et al. *Biased Cell Adhesion Organizes a Circuit for Visual Motion Integration*. <https://doi.org/10.1101/2023.12.11.571076> (2023).
71. Osaka, J. et al. *Complex Formation of Immunoglobulin Superfamily Molecules Side-IV and Beat-IIb Regulates Synaptic Specificity in the Drosophila Visual System*. (2023) <https://doi.org/10.1101/2023.03.27.534487>.
72. Zarin, A. A. et al. A transcription factor network coordinates attraction, repulsion, and adhesion combinatorially to control motor axon pathway selection. *Neuron* **81**, 1297–1311 (2014).
73. Venner, A. et al. An inhibitory lateral hypothalamic-preoptic circuit mediates rapid arousals from sleep. *Curr. Biol.* **29**, 4155–4168.e5 (2019).
74. O’Callaghan, E. K., Ballester Roig, M. N. & Mongrain, V. Cell adhesion molecules and sleep. *Neurosci. Res.* **116**, 29–38 (2017).
75. Zoghbi, H. Y. & Bear, M. F. Synaptic dysfunction in neurodevelopmental disorders associated with autism and intellectual disabilities. *Cold Spring Harb. Perspect. Biol.* **4**, a009886–a009886 (2012).
76. Micai, M. et al. Prevalence of co-occurring conditions in children and adults with autism spectrum disorder: A systematic review and meta-analysis. *Neurosci. Biobehav. Rev.* **155**, 105436 (2023).
77. Doldur-Balli, F. et al. Synaptic dysfunction connects autism spectrum disorder and sleep disturbances: A perspective from studies in model organisms. *Sleep. Med. Rev.* **62**, 101595 (2022).
78. Wang, Y. et al. The 3D Genome Browser: a web-based browser for visualizing 3D genome organization and long-range chromatin interactions. *Genome Biol.* **19**, 151 (2018).
79. Chen, S. et al. Light-dependent regulation of sleep and wake states by prokineticin 2 in zebrafish. *Neuron* **95**, 153–168.e6 (2017).
80. Lee, D., Oikonomou, G. & Prober, D. Large-scale Analysis of Sleep in Zebrafish. *BIO-PROTOCOL* **12**, (2022).
81. Malita, A. et al. A gut-derived hormone suppresses sugar appetite and regulates food choice in *Drosophila*. *Nat. Metab.* **4**, 1532–1550 (2022).
82. Matsliah, A. et al. Codex: Connectome Data Explorer. (2023).

Acknowledgements

We thank David Raizen, Amita Sehgal, members of the Kayser Lab, members of the Raizen Lab, and members of the Penn Chronobiology and Sleep Institute for helpful discussions and input. NIH T32GM008076 (K.M.), NIH T32HL007953 (KM), NIH T32HL007713 (A.Z.), NIH

R35HG011959 (A.C.). Fulbright Visiting Scholar Program—Postdoctoral Grant (FY-2017-TR-PD-07) (FDB). NIH P01HL160471 (A.I.P.). NIH R01HL143790 (S.F.G.). Daniel B. Burke Endowed Chair for Diabetes Research (S.F.A.G.). NIH DP2NS111996 (MSK). NIH R01NS120979 (M.S.K.). NIH R35NS137329 (M.S.K.). Linda Pechenik Montague Award (M.S.K.). Burroughs Wellcome Career Award for Medical Scientists (M.S.K.).

Author contributions

Conceptualization: K.M., A.Z., A.C., A.I.P., S.F.A.G., M.S.K. Investigation: K.M., A.Z., A.C., F.D.B., H.K., E.A.D.V., J.R. Writing—Original Draft: K.M., M.S.K. Writing—Review and Editing: K.M., A.Z., A.C., F.D.B., H.K., E.A.D.V., J.R., A.I.P., S.F.A.G., M.S.K. Project Supervision and Funding: M.S.K.

Competing interests

The authors declare no competing interests.

Additional information

Supplementary information The online version contains supplementary material available at <https://doi.org/10.1038/s41467-026-68343-1>.

Correspondence and requests for materials should be addressed to Matthew S. Kayser.

Peer review information *Nature Communications* thanks Junhai Han and the other anonymous reviewer(s) for their contribution to the peer review of this work. A peer review file is available.

Reprints and permissions information is available at <http://www.nature.com/reprints>

Publisher's note Springer Nature remains neutral with regard to jurisdictional claims in published maps and institutional affiliations.

Open Access This article is licensed under a Creative Commons Attribution-NonCommercial-NoDerivatives 4.0 International License, which permits any non-commercial use, sharing, distribution and reproduction in any medium or format, as long as you give appropriate credit to the original author(s) and the source, provide a link to the Creative Commons licence, and indicate if you modified the licensed material. You do not have permission under this licence to share adapted material derived from this article or parts of it. The images or other third party material in this article are included in the article's Creative Commons licence, unless indicated otherwise in a credit line to the material. If material is not included in the article's Creative Commons licence and your intended use is not permitted by statutory regulation or exceeds the permitted use, you will need to obtain permission directly from the copyright holder. To view a copy of this licence, visit <http://creativecommons.org/licenses/by-nc-nd/4.0/>.

© The Author(s) 2026